Terminal Molybdenum Phosphides with *d*-Electrons: Radical Character Promotes Coupling Chemistry

Joshua A. Buss, Paul H. Oyala, and Theodor Agapie*

Division of Chemistry and Chemical Engineering, California Institute of Technology, 1200 East California Boulevard, MC 127-72, Pasadena, California 91125, United States

Supporting Information

Contents

Experimental Details

General Considerations

Unless otherwise specified, all operations were carried out in an MBraun drybox under a nitrogen atmosphere or using standard Schlenk and vacuum line techniques. Solvents for air- and moisture-sensitive reactions were dried over sodium benzophenone ketyl, calcium hydride, or by the method of Grubbs.[1] Deuterated solvents were purchased from Cambridge Isotope Laboratories and vacuum transferred from sodium benzophenone ketyl (C_6D_6) or CaH_2 (CD_3CN). Solvents, once dried and degassed, were vacuum transferred directly prior to use or stored under inert atmosphere over activated 4 Å molecular sieves. **1**,[2] [P2Mo(MeCN)$_2$][2OTf],[2] **ClPA**,[3] **P$_2$A$_2$**,[3] Mg(THF)$_3$($C_{14}H_{10}$),[4] Me_2NPCl_2,[5] [Fc][BAr$^F{}_{24}$],[6] and [Fc][OTf][7] were prepared according to literature procedures. Unless indicated otherwise, all chemicals were used as received. PCl_3 (vacuum distilled from CaH_2), $HNMe_2$ (condensed trap-to-trap (0 °C to -78 °C)), HCl (4.0 M in dioxane), and PPh_4Cl (dried under vacuum at 40 °C, 12 h) were purchased from Sigma Aldrich. Anthracene was bought from Acros Organics. ^{1}H, ^{13}C{^{1}H}, and ^{31}P{^{1}H} NMR spectra were recorded on a Varian 400 MHz or Varian INOVA-500 spectrometers with shifts reported in parts per million (ppm). ^{1}H and ^{13}C{^{1}H} NMR spectra are referenced to residual solvent peaks.[8] ^{31}P{^{1}H} chemical shifts are referenced to an external 85% H_3PO_4 (0 ppm) standard. Multiplicities are abbreviated as follows: s = singlet, d = doublet, dd = doublet of doublets, ddd = doublet of doublet of doublets, t = triplet, vt = virtual triplet, m = multiplet, and br = broad. Elemental analysis was performed at the Caltech XRCF using a PerkinElmer 2400 Series II CHN Elemental Analyzer.

*Synthesis of **2***

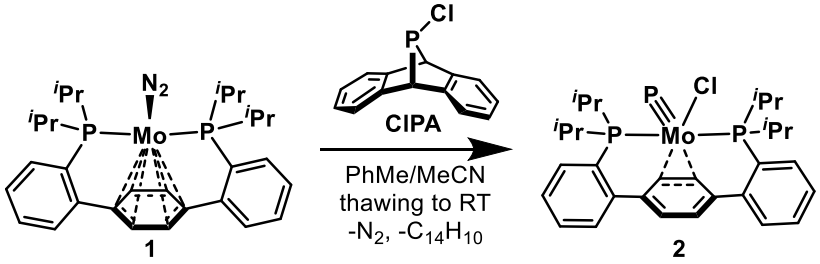

A 50 mL round bottom flask was charged with **1** (300 mg, 0.51 mmol), PhMe (5 mL), MeCN (2 mL), and a stir bar. After mixing for five minutes, the resulting red/brown solution was frozen in an LN_2 cooled cold well. A 20 mL scintillation vial was charged with a toluene solution of **ClPA** (137 mg, 0.56 mmol in 3 mL) and likewise frozen. The two solutions were combined, with stirring, immediately upon thawing. The round bottom was sealed and left to stir for one hour. At this time, the dark brown solution was dried *in vacuo*, providing a dark residue. Toluene was added to the residue which was transferred to a 20 mL scintillation vial and chilled to -35 °C for 8 hours. Collection of the resulting solids via vacuum filtration provided **2** as a black powder (212 mg, 0.34 mmol, 67% yield). Even after pumping on this powder for prolonged periods (>8 hours), a toluene solvent impurity persisted. Aside from this, the samples proved analytically pure. X-ray quality crystals of **2** could be grown by chilling a saturated toluene solution of **2** to -35 °C for two days or by slow diffusion of pentane into THF solutions of **2** at -35°C.

^{1}H (500 MHz, C_6D_6, 25 °C) δ: 7.33-7.36 (m, 4H, aryl-*H*), 7.15-7.19 (m, 4H, aryl-*H*), 5.86 (s, 2H, central arene-*H*), 5.46 (t, *J* = 2.8 Hz, 2H, central arene-*H*), 3.89-3.97 (m, 2H, C*H*(CH_3)$_2$), 2.69-2.77 (m, 2H, C*H*(CH_3)$_2$), 1.98-2.03 (m, 6H, CH(C*H*$_3$)$_2$), 1.51-1.55 (m, 6H, CH(C*H*$_3$)$_2$), 0.72-0.75 (m, 6H, CH(C*H*$_3$)$_2$), 0.16-0.20 (m, 6H, CH(C*H*$_3$)$_2$). ^{13}C{^{1}H} (126 MHz, C_6D_6, 25 °C) δ: 151.14 (vt, *J* = 6.5 Hz, aryl-*C*), 142.07 (vt, *J* = 4.7 Hz, central arene-*C*), 132.06 (s, aryl-*C*), 130.30 (s, aryl-*C*), 127.42 (vt, *J* = 2.3 Hz, aryl-*C*), 127.16 (vt, *J* = 2.8 Hz, aryl-*C*), 123.45 (vt, *J* = 13.9 Hz, aryl-*C*), 123.19 (s, central arene-*C*), 59.73 (vt, *J* =

3.5 Hz, central arene-*C*), 22.03 (vt, *J* = 7.5 Hz, *C*H(CH$_3$)$_2$), 21.36 (vt, *J* = 9.1 Hz, *C*H(CH$_3$)$_2$), 19.50 (br, CH(*C*H$_3$)$_2$), 17.71 (br, CH(*C*H$_3$)$_2$), 17.58 (br, CH(*C*H$_3$)$_2$), 15.81 (br, CH(*C*H$_3$)$_2$). ^{31}P{^{1}H} (162 MHz, C$_6$D$_6$, 23 °C) δ: 1300.73 (br t, Mo≡*P*), 41.27 (d, *J* = 11.1 Hz, *P*$_2$). Anal. Calcd. for **2•^{1}/$_2$PhMe** C$_{33.5}$H$_{44}$ClMoP$_3$ (%): C, 59.96; H, 6.61; N, 0.00 Found: C, 60.45, H, 6.29, N, <0.01.

*Synthesis of **3***

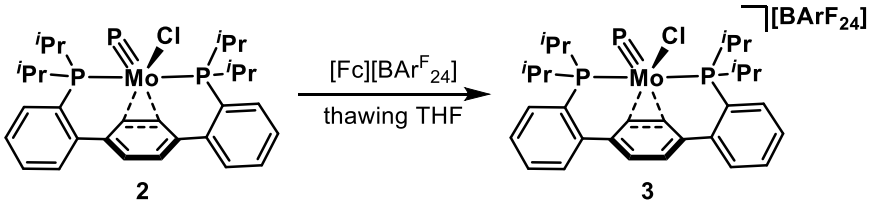

2 **3**

A 20 mL scintillation vial was charged with complex **2** (320 mg, 0.51 mmol) and a stir bar. THF (10 mL) was added and stirring was initiated, providing a red/brown solution. A second 20 mL scintillation vial was charged with a deep blue THF solution (10 mL) of [Fc][BAr$^F_{24}$] (539 mg, 0.51 mmol). Both vials were placed in an LN$_2$ cooled cold well and the contents frozen. Upon thawing, the solution of [Fc][BAr$^F_{24}$] was added dropwise to the solution of **2** with rapid stirring, resulting in an immediate color change to purple. Following the addition, the vial was returned to the cold well and to contents refrozen. The vial contents were allowed to thaw, mixed while cold, and then refrozen. This process was repeated four times, to facilitate complete oxidation of the starting material, and frozen a final time. A 125 mL Erlenmeyer flask charged with a stir bar, filled with pentane (100 mL), and placed in the cold well. Immediately upon thawing, the purple solution was added to the thawing pentane, with stirring, dropwise. A fine purple precipitate formed and the mixture was allowed to warm to room temperature. The solids were collected on a medium porosity frit, washed with hexanes (20 mL x 3), dried *in vacuo*, and collected as analytically pure **3** (710 mg, 0.48 mmol, 93%). X-ray quality crystals of **3** were obtained by vapor diffusion of pentane into a concentrated Et$_2$O solution at -35 °C. The Et$_2$O solution used for crystallization was prepared and filtered while cold to prevent further reactivity of complex **3**.

Phosphide Oxidation Reactions

*Formation of **4***

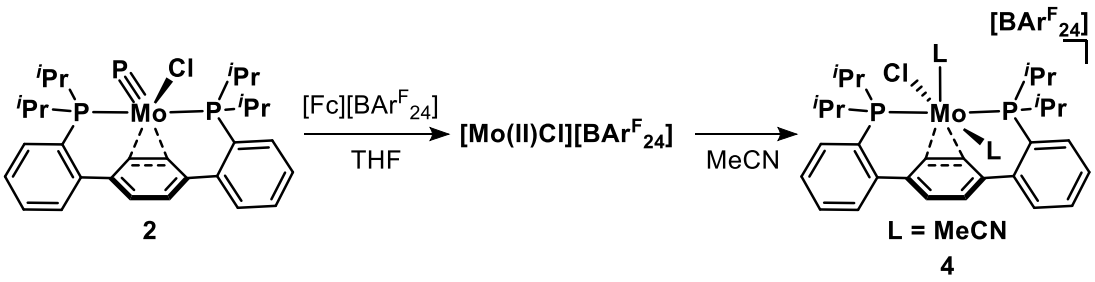

2 **4**

In a typical reaction, a 20 mL scintillation vial was charged with a THF (10 mL) solution of **2** (239 mg, 0.38 mmol) and a stir bar. The vial was placed in an LN_2 chilled cold well and the contents frozen. While thawing, a thawing solution of [Fc][BAr$^F_{24}$] (400 mg, 0.38 mmol) in THF (6 mL) was added dropwise, with stirring. This addition resulted in an immediate color change to deep purple. Upon warming to room temperature, the color changed to a red/brown. An aliquot of the reaction mixture at this juncture showed clean conversion to a single diamagnetic $^{31}P\{^1H\}$ NMR resonance at 76.3 ppm. The THF was removed under reduced pressure and the resulting residue triturated with hexanes (3 mL), providing a brown foamy solid. These solids were suspended in hexanes (6 mL) and filtered through celite. The filter cake was washed with a 3:1 mixture of hexanes and benzene (*ca.* 8 mL x 3) until the washes were colorless. The filter cake was extracted with Et_2O (10 mL) and solvent was removed *in vacuo*, affording a tacky brown residue. The ^1H and $^{31}P\{^1H\}$ NMR spectra of this material in CD_3CN are consistent with a single diamagnetic metal complex, **4**. The BAr$^F_{24}$ salt of **4** eluded crystallization, but repeating the above procedure with [Fc][OTf] in lieu of [Fc][BAr$^F_{24}$] and extracting the filter cake with MeCN (5 mL) rather than Et_2O afforded the OTf salt of **4**. Single crystals of this complex were obtained from slow diffusion of Et_2O into a concentrated MeCN solution of **4** at -35 °C.

^1H (400 MHz, CD_3CN, 21 °C) δ: 7.73 (br, 8H, BAr$^F_{24}$ *ortho-H*), 7.69 (br, 4H, BAr$^F_{24}$ *para-H*), 7.56-7.61 (m, 4H, aryl-*H*), 7.51-7.54 (m, 2H, aryl-*H*), 7.39-7.41 (m, 2H, aryl-*H*), 5.20 (t, *J* = 3.81 Hz, 4H, central arene-*H*), 3.24 (br m, 4H, C*H*(CH_3)$_2$), 1.22-1.29 (m, 24H, CH(C*H*$_3$)$_2$). ^{31}P (162 MHz, CD_3CN, 21 °C) δ: 69.26 (s).

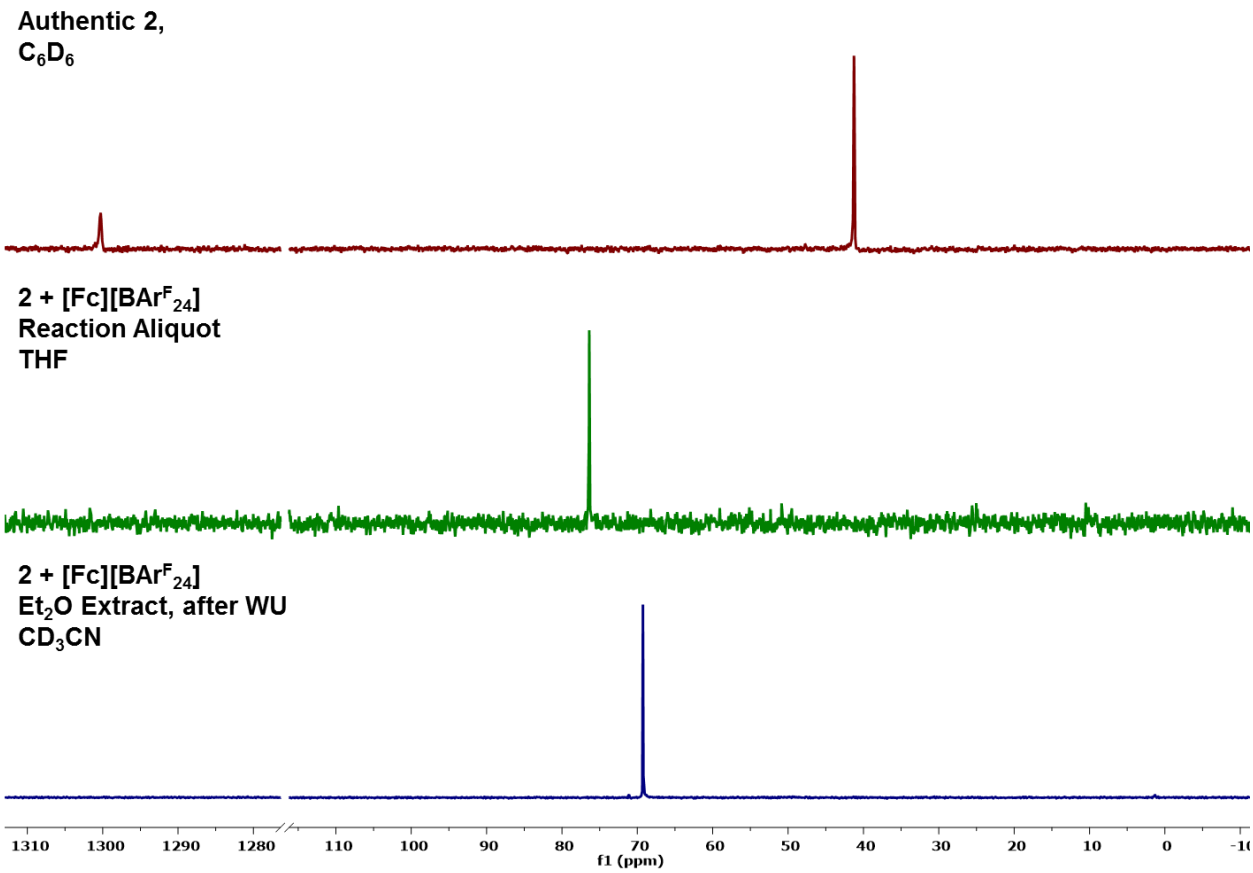

Figure S1—Partial $^{31}P\{^{1}H\}$ NMR spectra tracking the one electron oxidation of **2**. A single resonance at 76.3 ppm is observed upon oxidation in THF (assigned to [Mo(II)Cl][BAr^{F}_{24}], Figure S1 middle) which shifts upfield to 69.3 ppm upon addition of MeCN. This species has been confirmed by single crystal XRD and independent synthesis as the bis(acetonitrile) chloride cation, **4**.

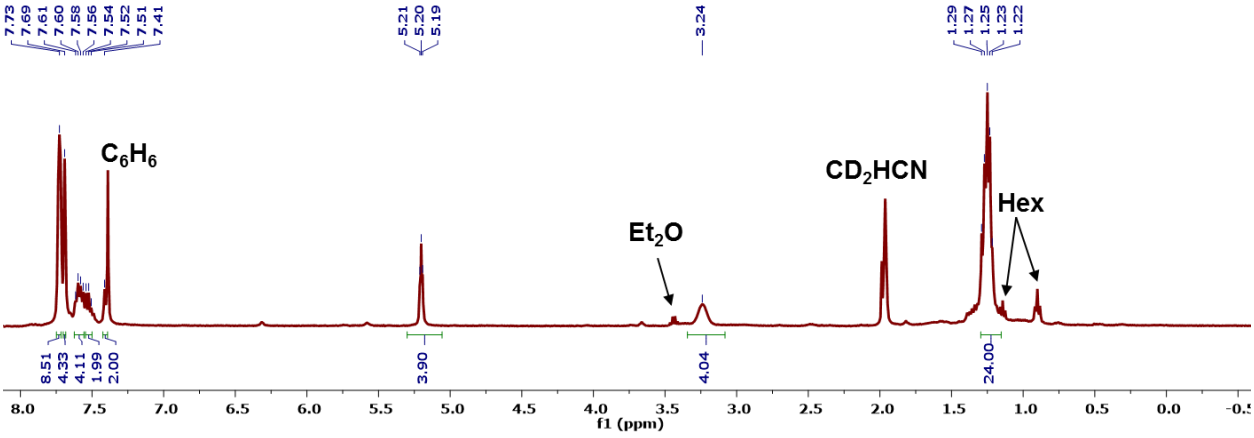

Figure S2—^{1}H NMR Spectrum (400 MHz, CD_3CN, 21°C) of **4**.

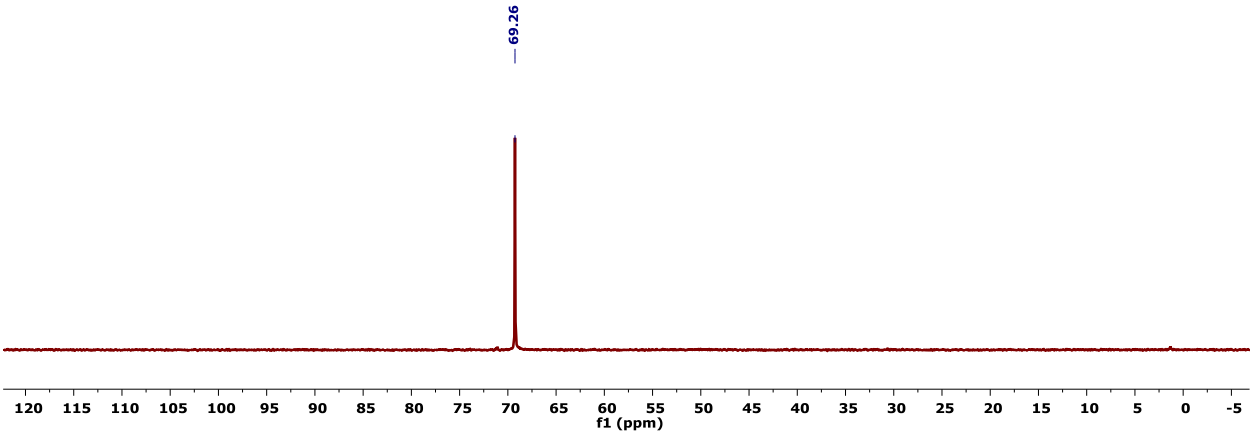

Figure S3—$^{31}P\{^{1}H\}$ NMR Spectrum (126 MHz, CD_3CN, 21°C) of **4**.

*Independent Preparation of **4***

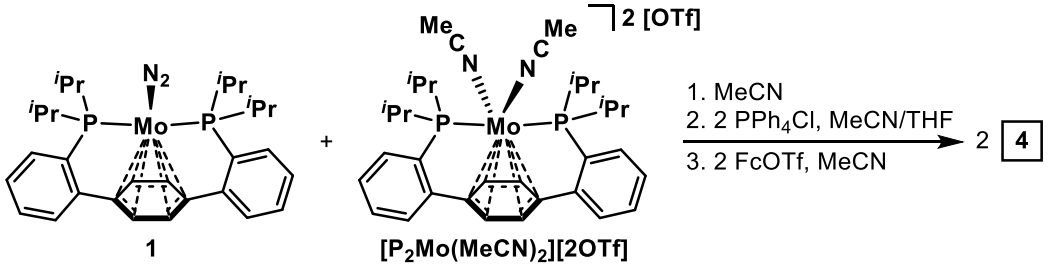

To confirm the identity of complex **4**, an independent preparation was performed according to the scheme above. A 20 mL scintillation vial was charged with **1** (200 mg, 0.34 mmol) and a stir bar. MeCN (5 mL) was added, resulting in a dark brown heterogeneous mixture. A MeCN (5 mL) solution of [P2Mo(MeCN)$_2$][2OTf] (320 mg, 0.33 mmol) was added dropwise, resulting in a color change to deep green. Solvent was removed *in vacuo* and the resulting green solids were suspended in Et_2O and filtered, washing away unreacted **1**. The filter cake was extracted with MeCN and volatiles were removed under reduced pressure. The resulting green residue was triturated with Et_2O, providing a pale green powder that was used without further purification or characterization.

To a THF (4 mL) solution of the green residue in a 20 mL scintillation vial charged with a stir bar, a MeCN (3 mL) solution of PPh_4Cl (25 mg, 0.067 mmol) was added with stirring. An immediate color change to red/orange was observed and the reaction was left to stir for 3 h. At this time, volatiles were removed *in vacuo* and the resulting solids triturated with hexanes, providing an orange powder. Benzene was added and the resulting mixture filtered through celite. The filtrate was lyophilized, affording an orange powder that was used without further purification or characterization.

A J. Young NMR tube was charged with the aforementioned orange powder (20 mg, 0.034 mmol), [Fc][OTf] (11 mg, 0.034 mmol), and CD_3CN (0.6 mL). Upon dissolution of the starting materials, the color darkened to red/brown. ^{1}H and $^{31}P\{^{1}H\}$ NMR spectroscopy of the reaction mixture was consistent with formation of chloride cation **4**.

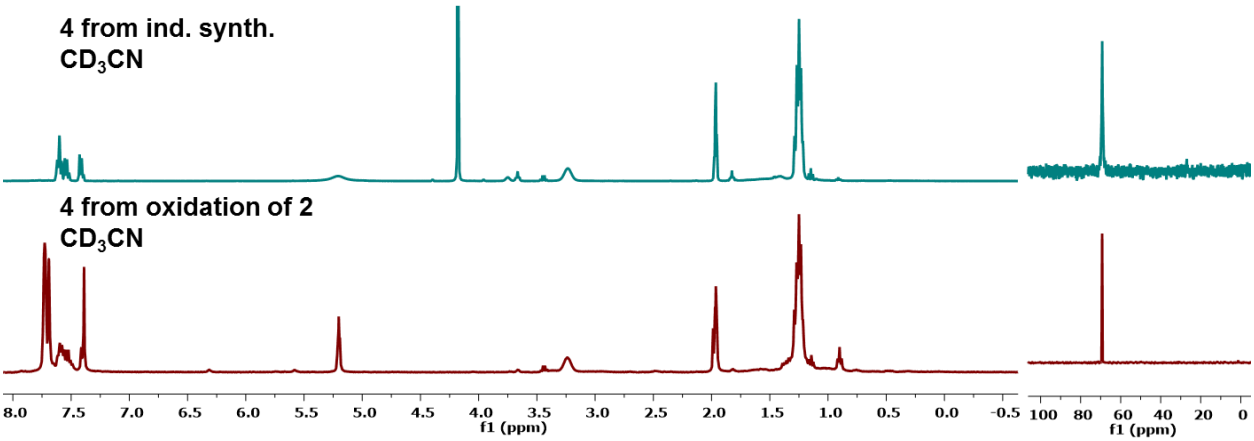

Figure S4—^{1}H NMR Spectra (400 MHz, CD_3CN, 21°C—left) and $^{31}P\{^{1}H\}$ NMR spectra (126 MHz, CD_3CN, 21 °C—right) of complex **4** prepared via sequential conproportionation, chlorination, and oxidation (top) and phosphide oxidation (bottom).

Formation of 5

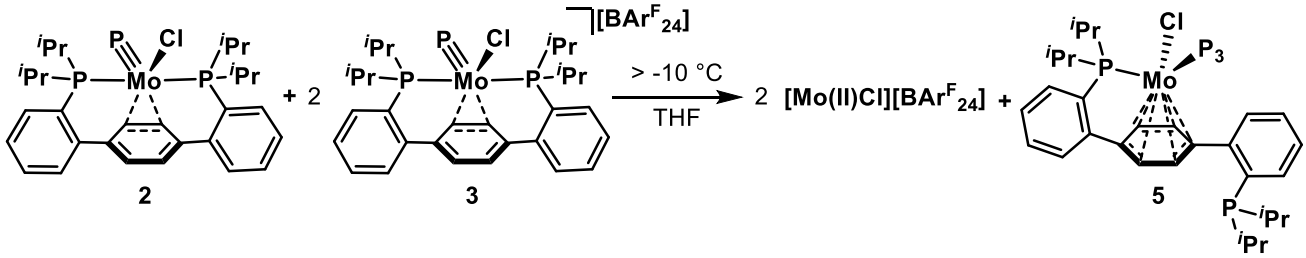

A 20 mL scintillation vial was charged with **3** (120 mg, 0.081 mmol) and a stir bar. The vial was placed in a LN_2 cooled cold well and the solids were cooled for 5 min. At this time, thawing THF (5 mL) was added, providing a deep purple solution. The vial was returned to the cold well and the solution frozen. Complex **2** (26 mg, 0.041 mmol) was added as a solid and the reaction mixture left to thaw, with stirring. After stirring at room temperature for 30 min, the volatiles were removed under reduced pressure, providing a brown residue. This residue was suspended in hexanes (5 mL) and filtered through Celite. The filter cake was extracted with hexanes (5 mL x 3) and these washes were combined. The remaining solids were washed with Et_2O until the filtrate was colorless. Both filtrate solutions were dried *in vacuo*, providing mixtures primarily comprised of free *para*-terphenyl diphosphine, **2**, and **5** (hexane wash, Figure S5, middle) and **5**, a Mo(II) chloride cation (which upon MeCN addition forms **4**), and a paramagnetic impurity (Et_2O wash, Figure S5, bottom).

^{1}H (500 MHz, C_6D_6, 25 °C) δ: 8.08-8.09 (br m, 1H, aryl-*H*), 7.49 (br d, *J* = 6.04 Hz, 1H, aryl-*H*), 7.20-2.21 (m, 1H, aryl-*H*; overlaps with residual C_6D_5H but corroborated by 2D NMR), 7.11 (br dd, *J* = 7.83 Hz, 1H, aryl-*H*; overlaps with residual C_6D_5H but corroborated by 2D NMR), 7.01 (br dd, *J* = 6.71 Hz, 1H, aryl-*H*), 6.89 (br m, 2H, aryl-*H*), 6.77 (br m, 1H, aryl-*H*), 5.34 (br s, 1H, central arene-*H*), 5.25 (br d, *J* = 6.53 Hz, 1H, central arene-*H*), 4.58 (br d, *J* = 3.73 Hz, 1H, central arene-*H*), 4.20 (br s, 1H, central arene-*H*), 3.70-3.76 (m, 1H, C*H*$(CH_3)_2$), 3.03-3.09 (m, 1H, C*H*$(CH_3)_2$), 2.82-2.89 (m, 1H, C*H*$(CH_3)_2$), 2.40-2.49 (m, 1H, C*H*$(CH_3)_2$), 1.98-2.03 (m, 1H, CH(C*H*$_3)_2$), 1.69-1.74 (m, 1H, CH(C*H*$_3)_2$), 1.38-1.43 (m, 1H, CH(C*H*$_3)_2$; overlaps with residual THF but corroborated by 2D NMR), 1.03-1.09 (m, 1H, CH(C*H*$_3)_2$), 0.85-0.88 (m, 1H, CH(C*H*$_3)_2$; overlaps with *para*-terphenyl diphosphine impurity but corroborated by 2D NMR), 0.47-0.52 (m, 1H, CH(C*H*$_3)_2$), 0.28-0.32 (m, 1H, CH(C*H*$_3)_2$). $^{13}C\{^{1}H\}$ (126 MHz, C_6D_6, 25 °C) δ: 148.78-148.89

(m, aryl-*C*), 145.95 (d, *J* = 8.08 Hz, aryl-*C*), 133.78 (s, aryl-*C*), 132.63 (s, aryl-*C*), 131.61 (d, *J* = 2.63 Hz, aryl-*C*), 131.03 (d, *J* = 4.93 Hz, aryl-*C*), 130.25 (s, aryl-*C*), 129.90 (s, aryl-*C*), 129.73 (s, aryl-*C*), 128.85 (s, aryl-*C*; overlaps with residual C_6D_6 but corroborated by 2D NMR), 126.20 (d, *J* = 9.53 Hz, aryl-*C*), 123.08 (s, central arene-*C*), 106.46 (s, central arene-*C*), 94.11 (d, *J* = 16.59 Hz, central arene-*C*), 90.85 (d, *J* = 3.48 Hz, central arene-*C*), 85.95 (d, *J* = 2.06 Hz, central arene-*C*), 29.17 (d, *J* = 19.47 Hz, *C*H(CH$_3$)$_2$), 27.68 (m, *C*H(CH$_3$)$_2$), 25.09 (m, *C*H(CH$_3$)$_2$), 23.26 (br s, *C*H(CH$_3$)$_2$), 20.36 (s, CH(*C*H$_3$)$_2$), 20.23 (s, CH(*C*H$_3$)$_2$), 19.31 (d, *J* = 9.60 Hz, CH(*C*H$_3$)$_2$), 18.33 (s, CH(*C*H$_3$)$_2$), 18.16 (s, CH(*C*H$_3$)$_2$), 18.08 (d, *J* = 2.67 Hz, CH(*C*H$_3$)$_2$), 17.73 (s, CH(*C*H$_3$)$_2$), 17.58 (d, *J* = 6.55 Hz, CH(*C*H$_3$)$_2$), 16.99 (m, CH(*C*H$_3$)$_2$). $^{31}P\{^1H\}$ (162 MHz, C_6D_6, 23 °C) δ: 65.75 (d, *J* = 17.04 Hz, Mo-*P*$_{diphosphine}$), -4.62 (s, *P*$_{diphoshine}$), -162.35 (dd, *J* = 314.71 and 264.90 Hz, *P*$_3$), -204.70 (t, *J* = 264.90 Hz, *P*$_3$), -306.93 (ddd, *J* = 314.71, 264.90, and 17.04 Hz, *P*$_3$).

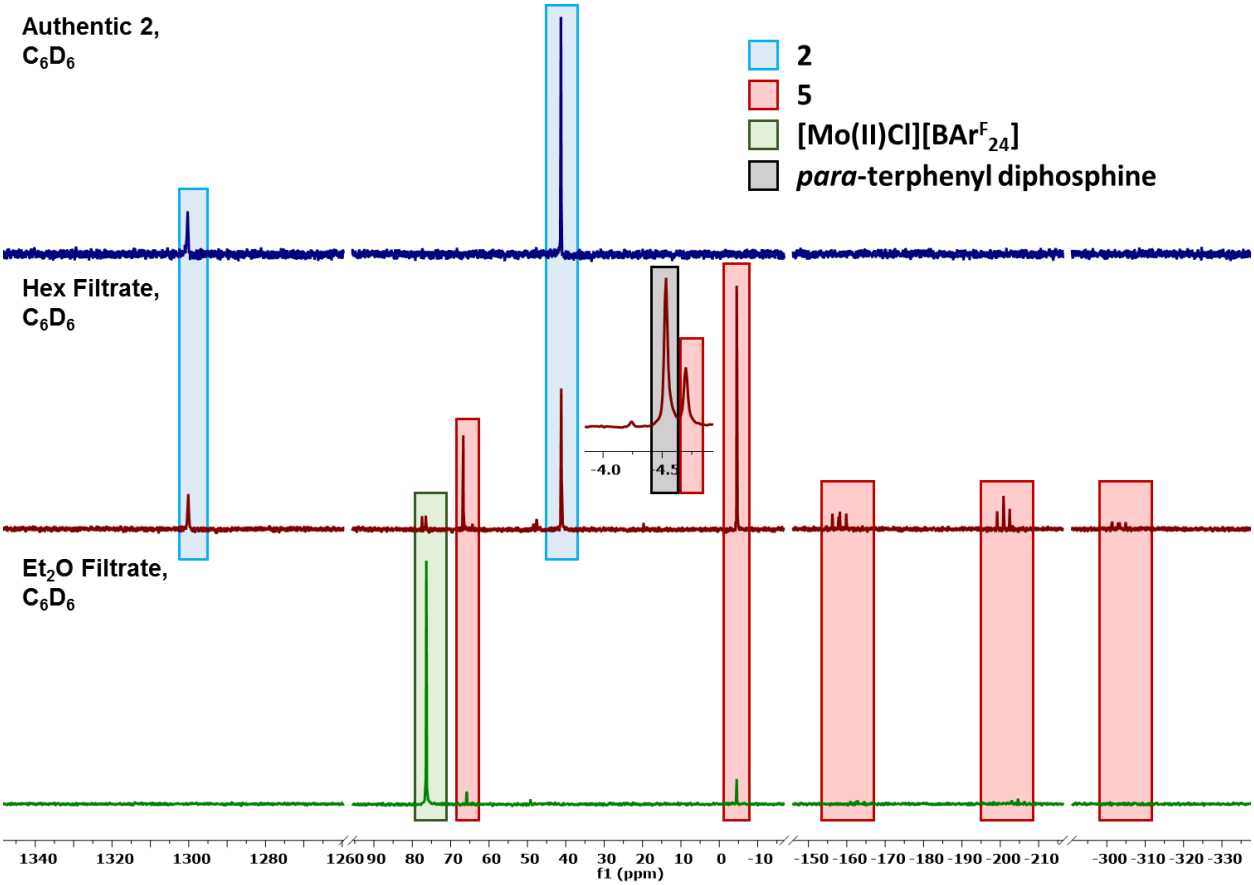

Figure S5—Partial $^{31}P\{^1H\}$ NMR spectra (126 MHz, C_6D_6, 25 °C) of an authentic sample of **2** (top), the hexane extract of a reaction between **2** and **3** (middle), and the diethyl ether extract of the same reaction (bottom).

Independent Synthesis of ***5***

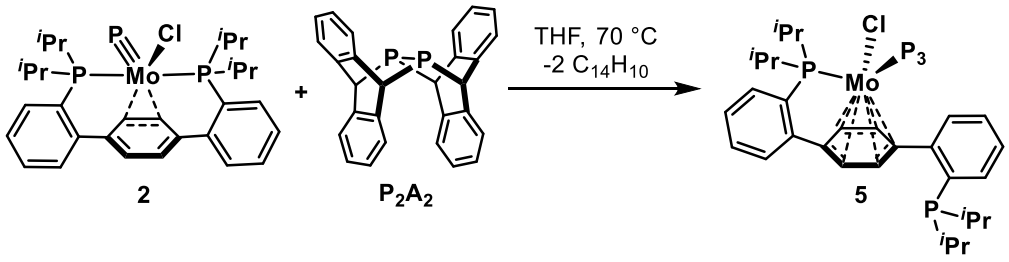

A J. Young NMR tube was charged with **2** (24 mg, 0.039 mmol), $\mathbf{P_2A_2}$ (17 mg, 0.039 mmol), and THF (600 µL). A $^{31}P\{^{1}H\}$ NMR spectrum of the resulting red/brown solution was recorded (Figure S6, top). The J. Young tube was placed in an oil bath pre-heated to 70 °C for 3 h. A second $^{31}P\{^{1}H\}$ NMR spectrum was collected at this time, demonstrating consumption of $\mathbf{P_2A_2}$, as well as a mixture of **2**, **5**, P_4, and free *para*-terphenyl diphosphine (Figure S6, bottom).

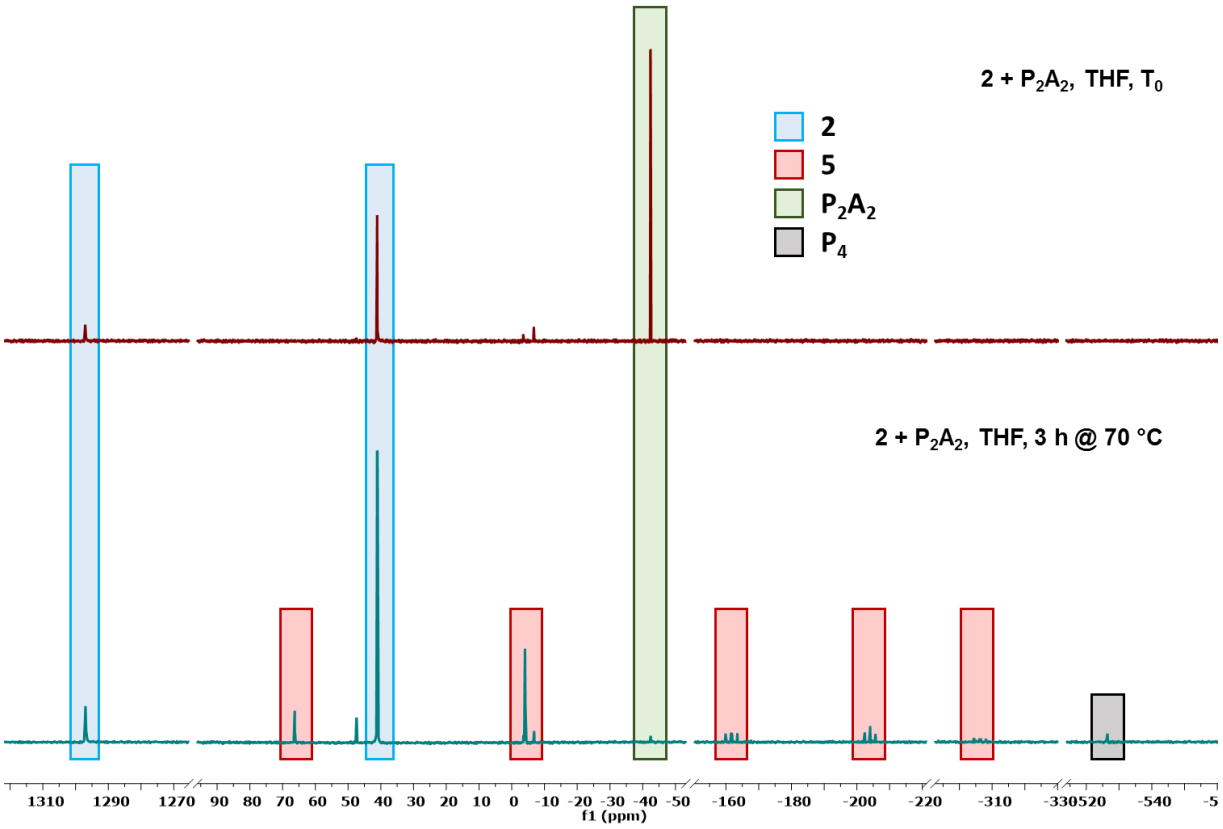

Figure S6—Partial $^{31}P\{^{1}H\}$ NMR spectra (126 MHz, THF, 25 °C) of a 1:1 mixture of **2** and $\mathbf{P_2A_2}$ prior to (top) and following (bottom) heating to 70 °C.

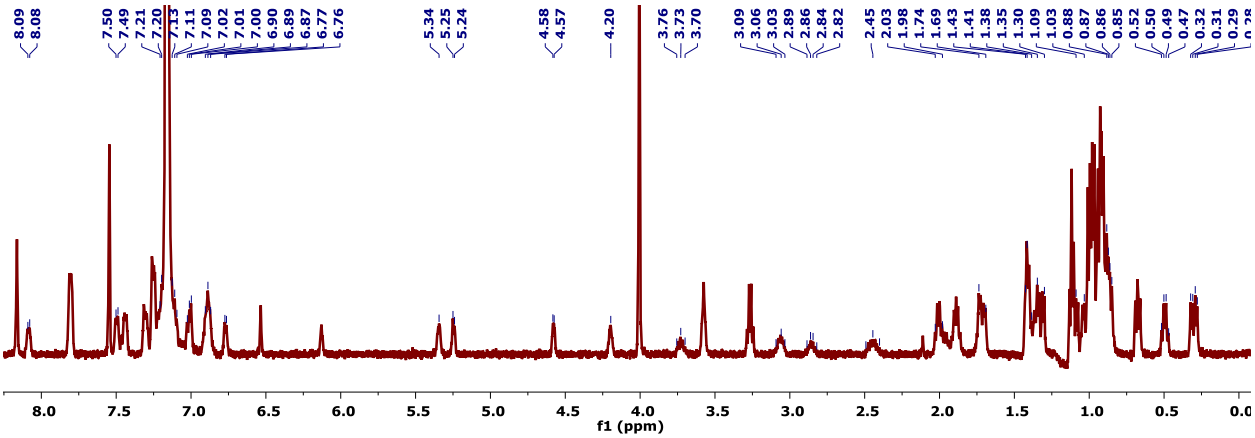

Figure S7—^{1}H NMR Spectrum (400 MHz, C_6D_6, 25°C) of a mixture containing **5** as the major component. Only the resonances corresponding to **5** are labeled.

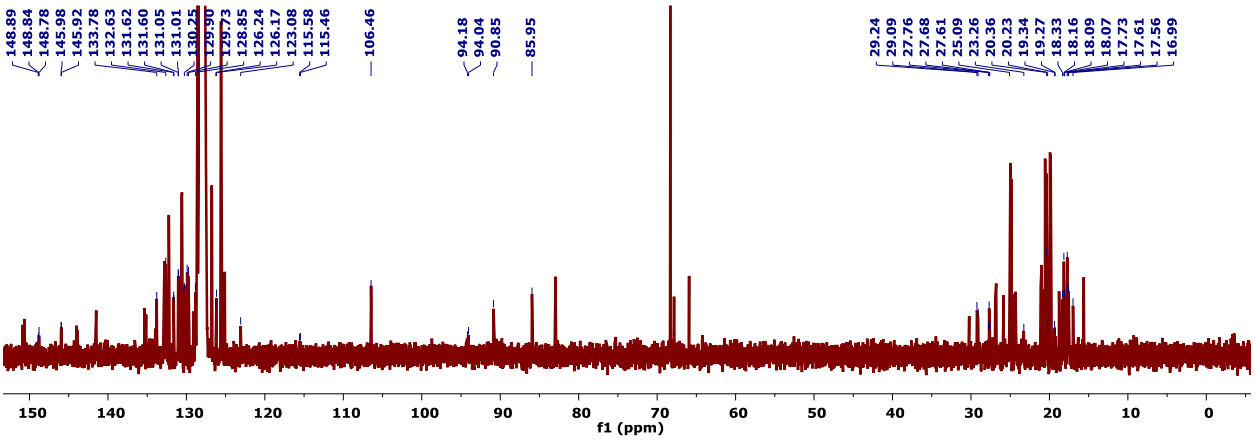

Figure S8—^{13}C{^{1}H} NMR Spectrum (126 MHz, C_6D_6, 25°C) of a mixture containing 5 as the major component. Only the resonances corresponding to **5** are labeled.

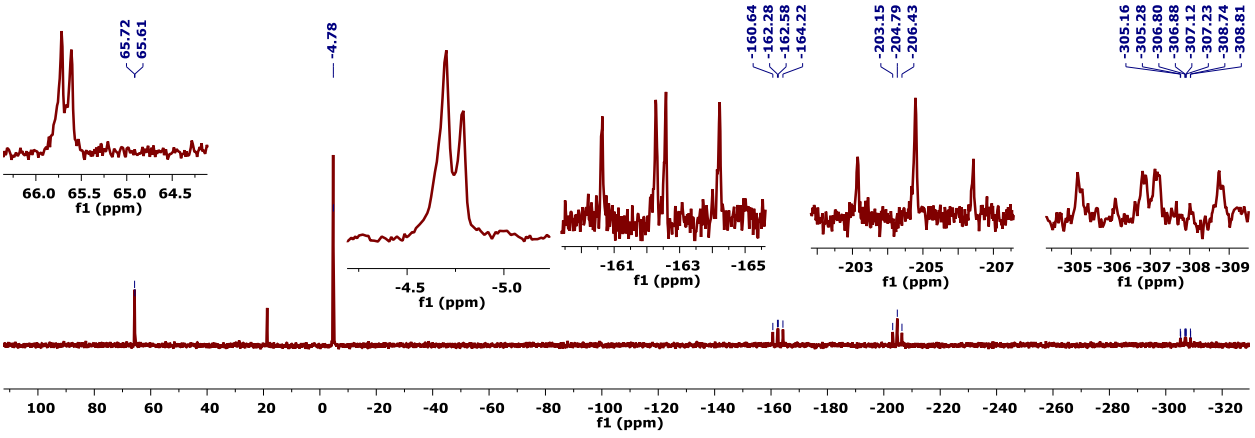

Figure S9—^{31}P{^{1}H} NMR Spectrum (162 MHz, C_6D_6, 23°C) of a mixture containing **5** as the major component. Only the resonances corresponding to **5** are labeled.

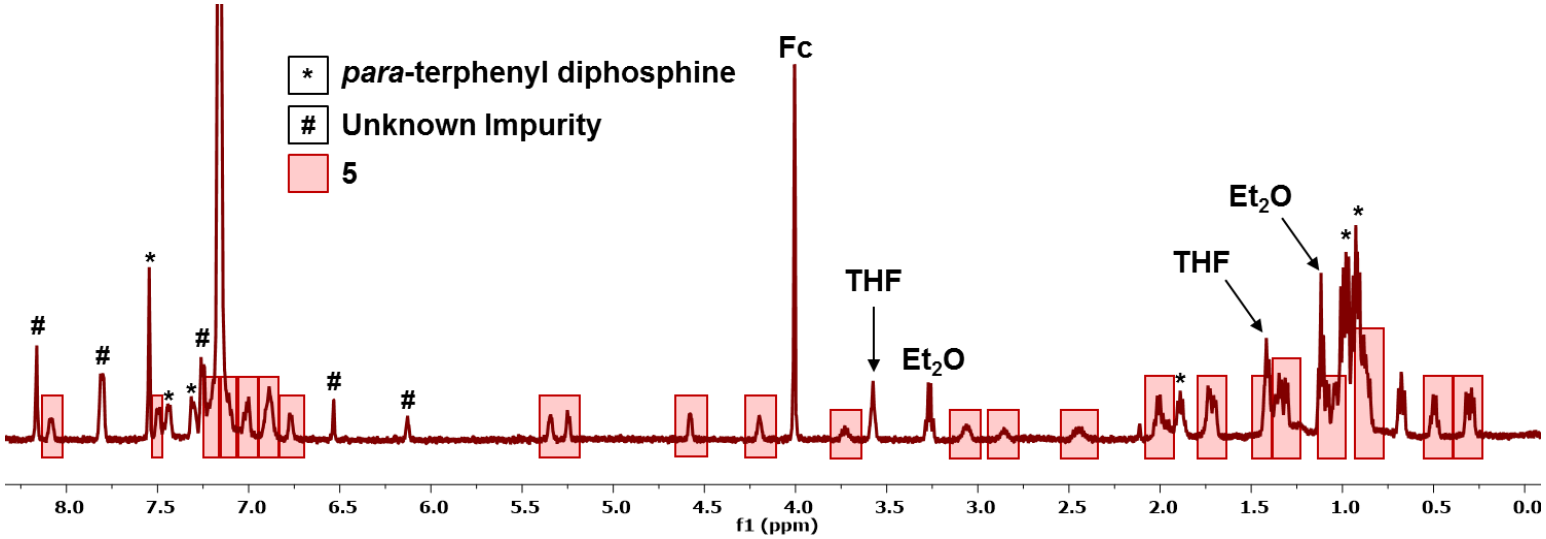

Figures S10—^{1}H NMR Spectrum (500 MHz, C_6D_6, 25°C) of a mixture containing **5** as the major component. All resonances have been assigned, with those corresponding to complex **5** emphasized in red.

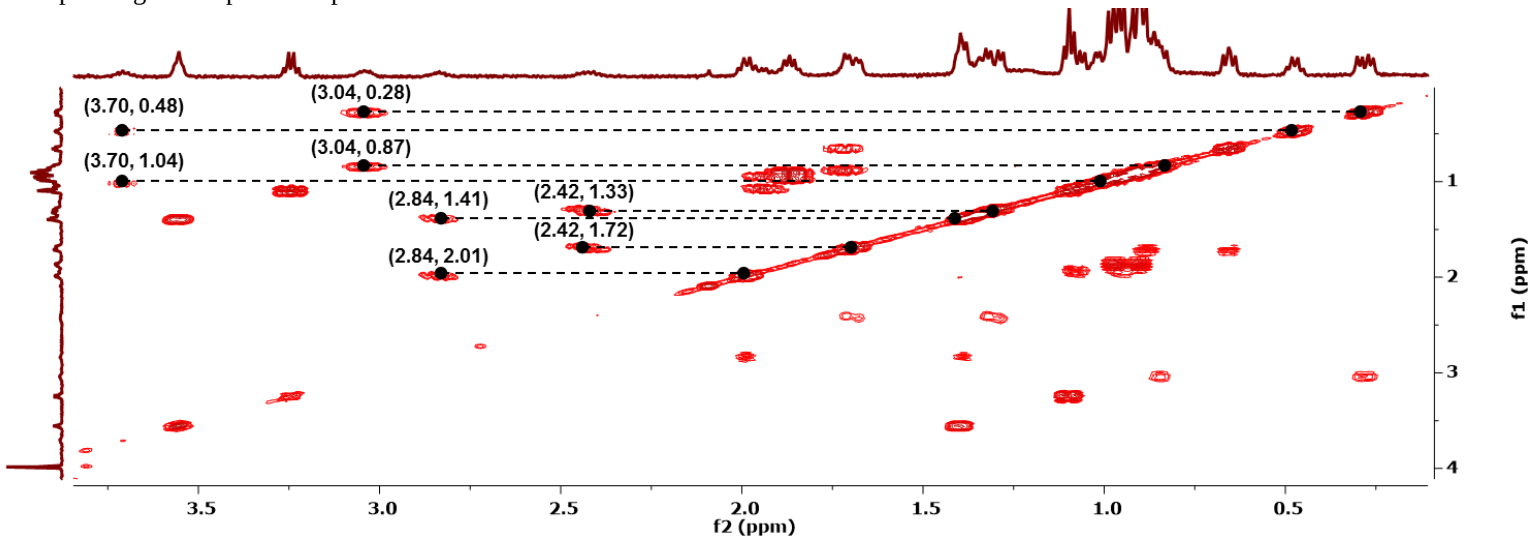

Figure S11— Partial ^{1}H/^{1}H COSY NMR Spectrum (500 MHz, C_6D_6, 25°C) of mixture containing **5** as the major component. The scalar coupling correlations between the isopropyl methine and isopropyl methyl resonances are labeled.

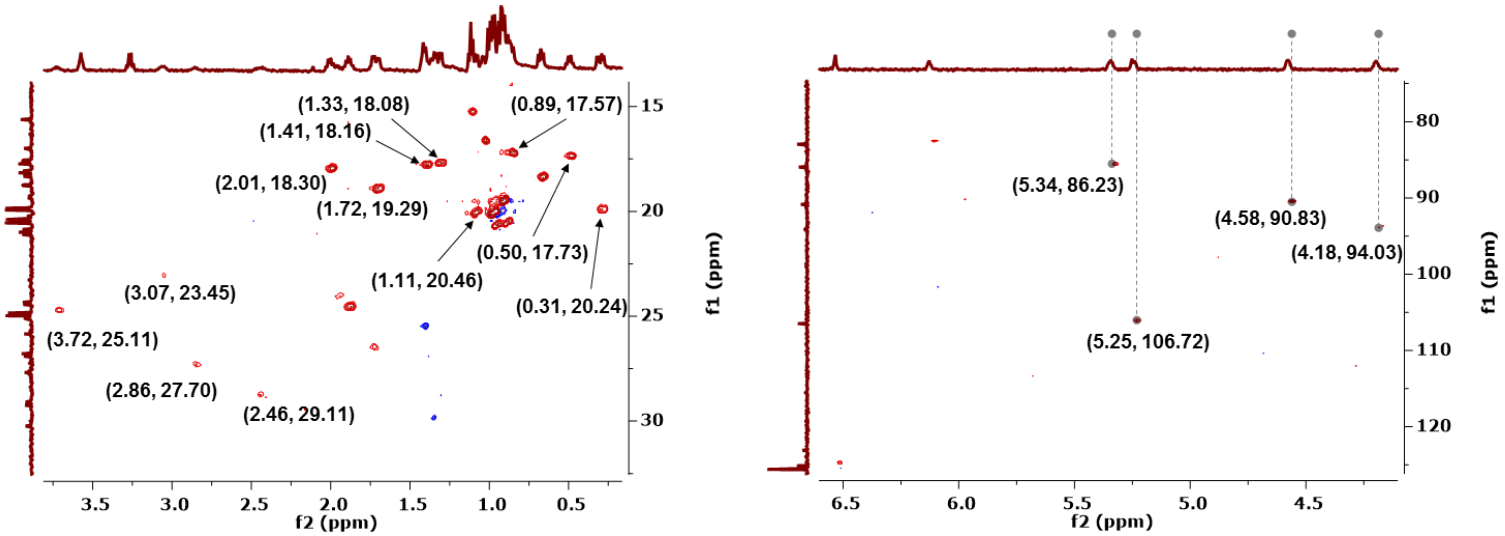

Figure S12—Partial $^{1}H/^{13}C$ HSQC NMR Spectra (500/126 MHz, C_6D_6, 25°C) of mixture containing **5** as the major component. Cross peaks corresponding to the aliphatic (left) and central arene (center) ^{1}J(C,H) correlations are labeled.

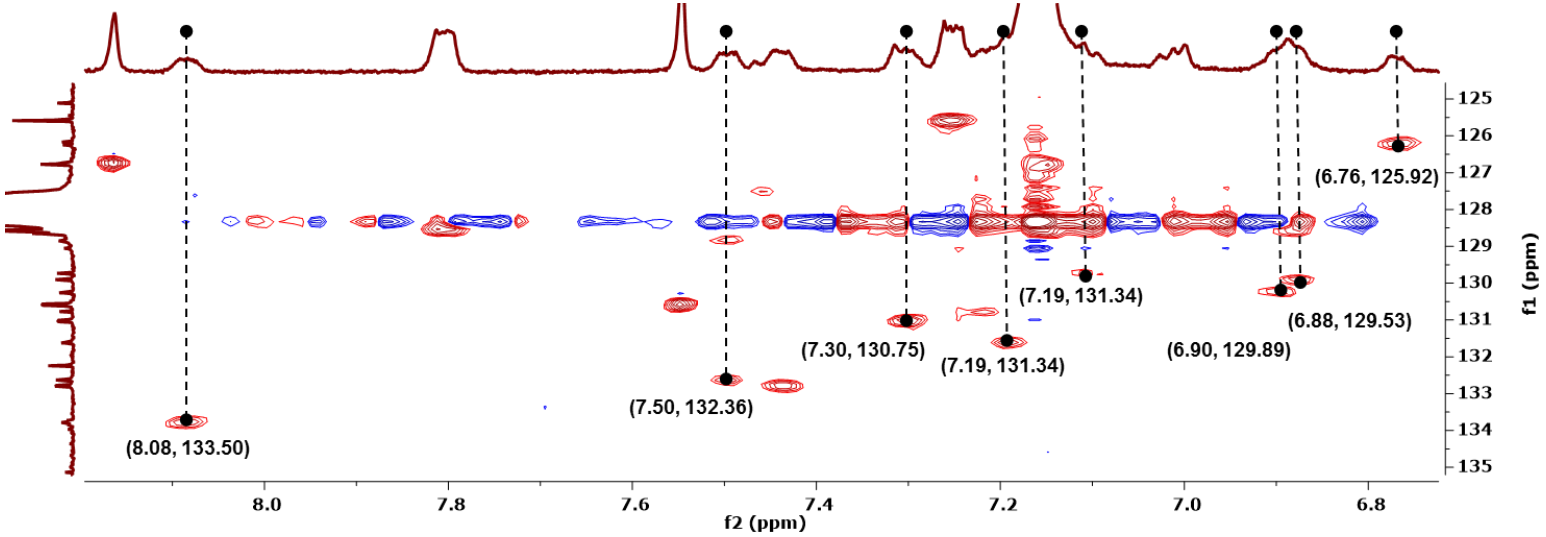

Figure S13— Partial $^{1}H/^{13}C$ HSQC NMR Spectrum (500/126 MHz, C_6D_6, 25°C) of a mixture containing **5** as the major component.

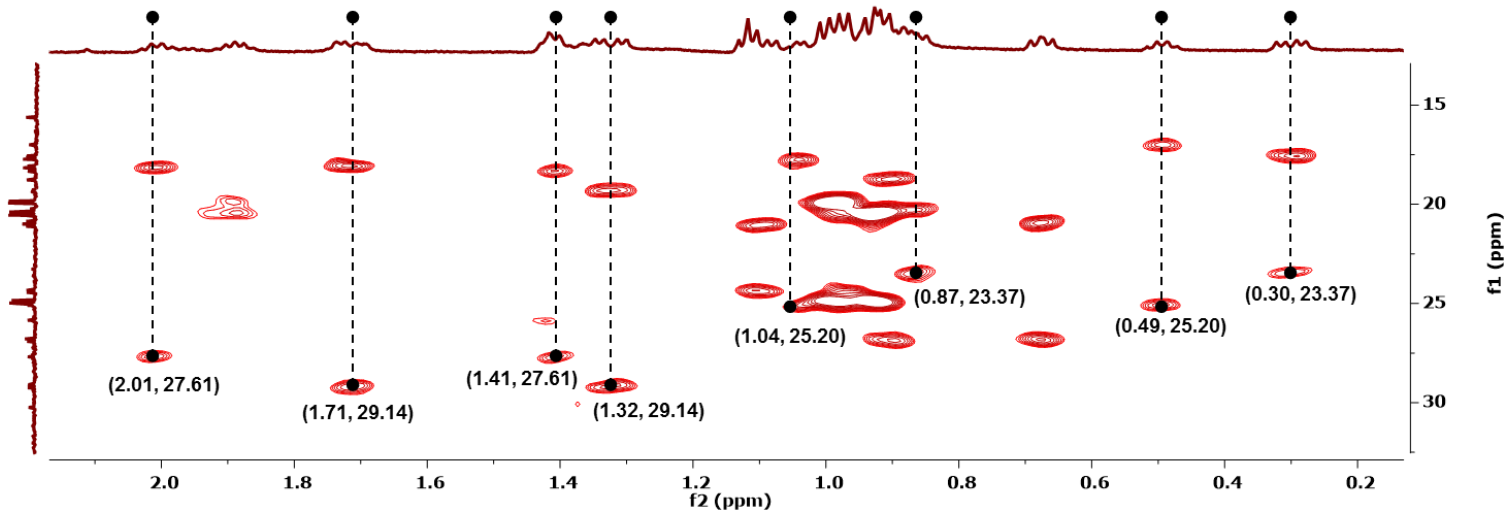

Figure S14—Partial $^{1}H/^{13}C$ HMBC NMR Spectrum (500/126 MHz, C_6D_6, 25°C) of a mixture containing **5** as the major component.

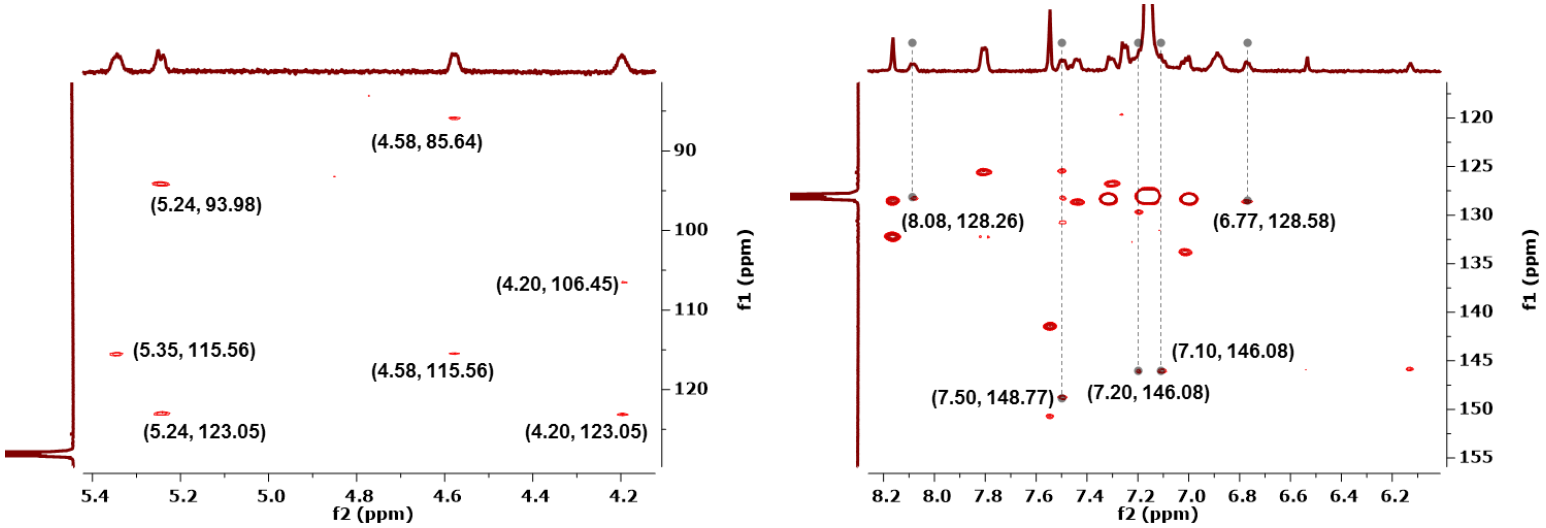

Figure S15— Partial $^{1}H/^{13}C$ HMBC NMR Spectrum (500/126 MHz, C_6D_6, 25°C) of a mixture containing **5** as the major component. The central arene (left) and phenylene (right) $^{2/3}J$(C,H) scalar coupling correlations are labeled.

NMR Spectra

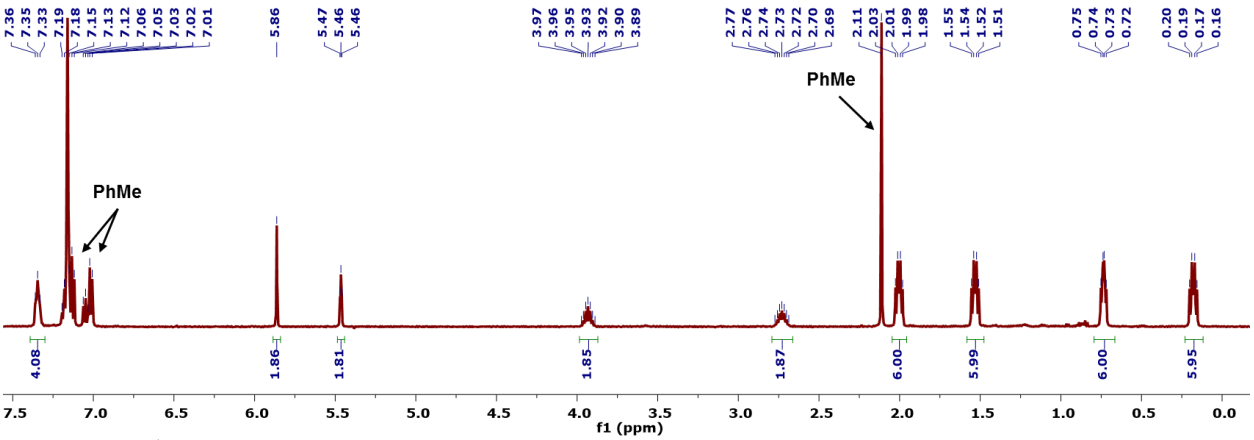

Figure S16—^{1}H NMR Spectrum (500 MHz, C_6D_6, 25°C) of **2**.

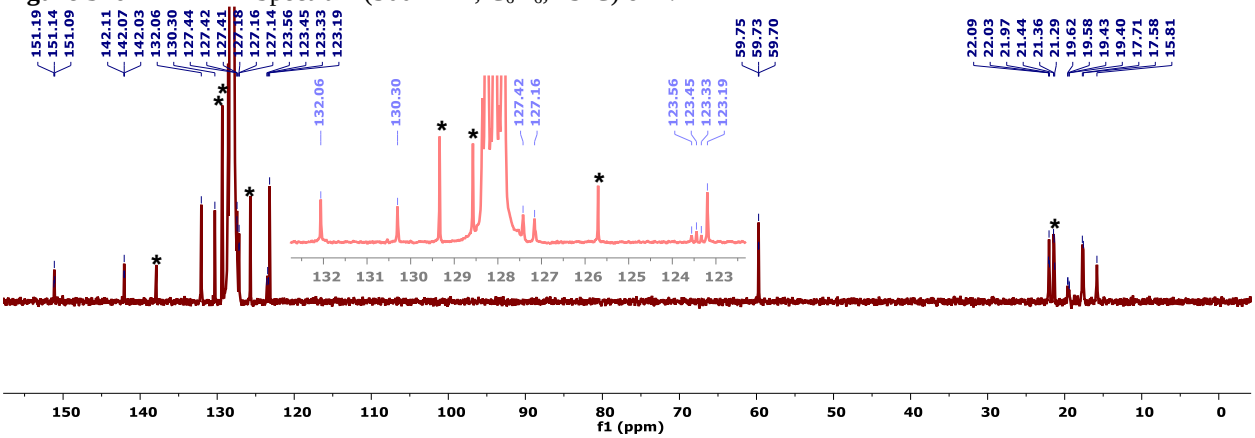

Figure S17—^{13}C{^{1}H} NMR Spectrum (126 MHz, C_6D_6, 25°C) of **2**. The inset shows an enlargement of the aryl resonances near the C_6D_6 solvent residual. ^{13}C NMR signals corresponding to toluene are denoted with an asterisk.

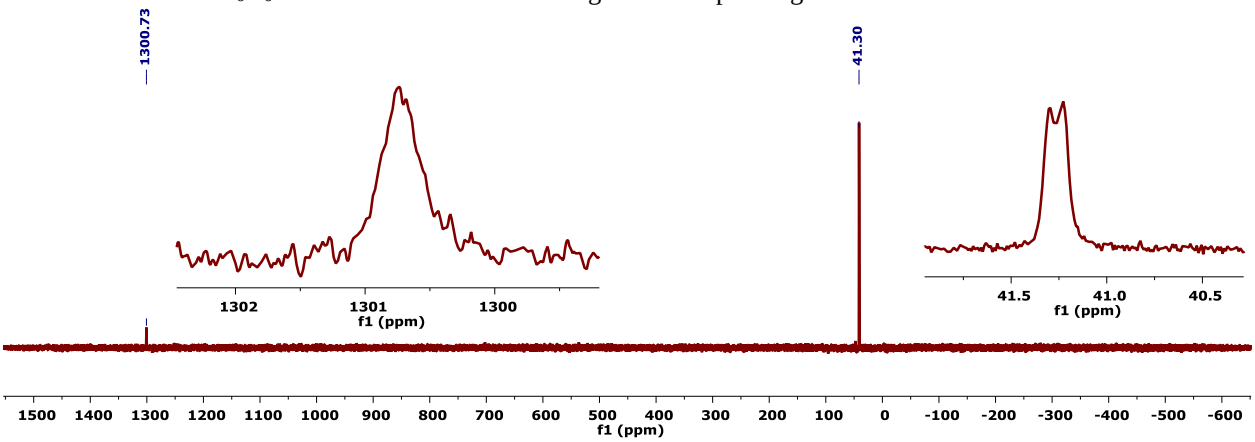

Figure S18—^{31}P{^{1}H} NMR Spectrum (162 MHz, C_6D_6, 23°C) of **2**. The insets show enlargements of the phosphide (left) and phosphine (right) resonances, demonstrating a broad signal for the former and a broad, but resolved, doublet for the latter.

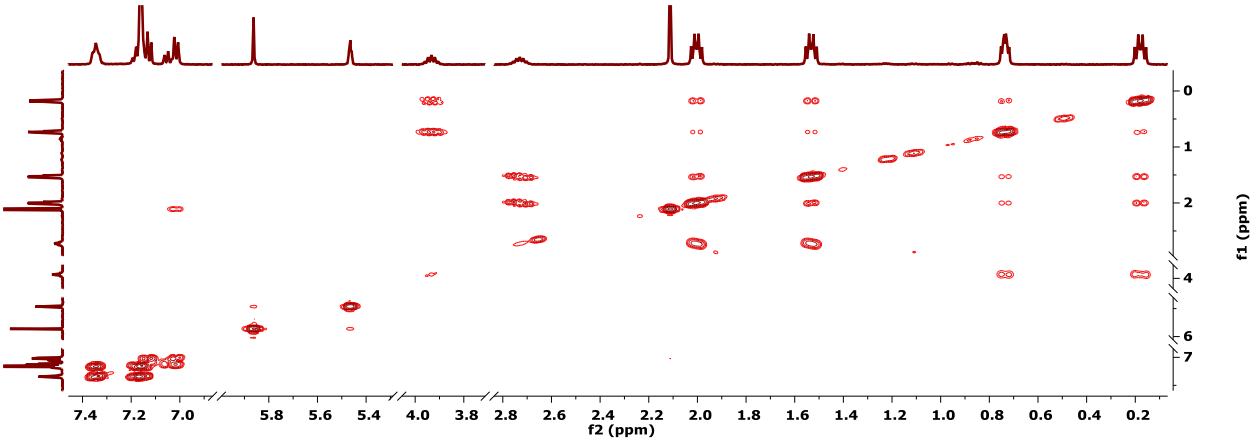

Figure S19—Partial $^{1}H/^{1}H$ COSY NMR Spectrum (500 MHz, C_6D_6, 25°C) of **2**.

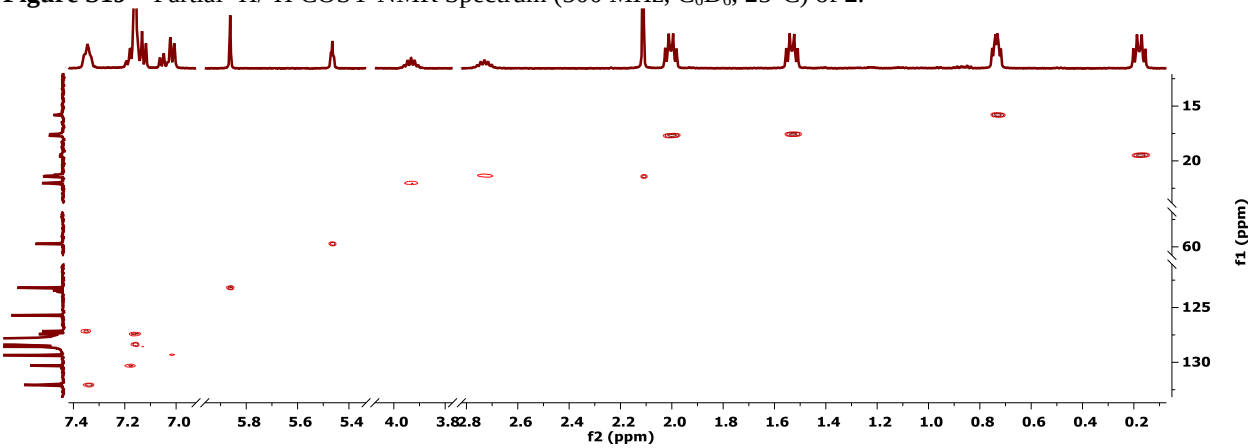

Figure S20—Partial $^{1}H/^{13}C$ HSQC NMR Spectrum (500/126 MHz, C_6D_6, 25°C) of **2**.

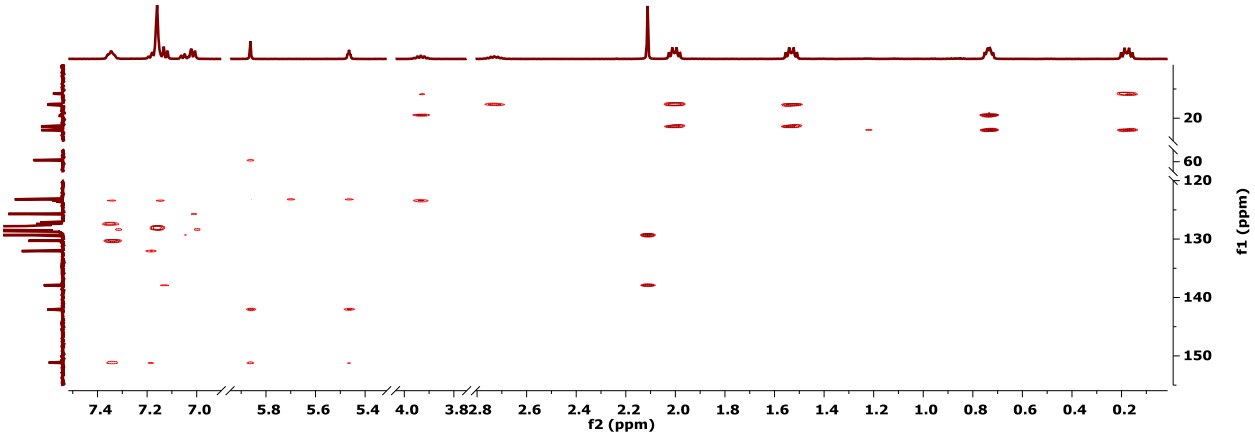

Figure S21—Partial $^{1}H/^{13}C$ HMBC NMR Spectrum (500/126 MHz, C_6D_6, 25°C) of **2**.

EPR Spectroscopy

Experimental Details

CW EPR Spectroscopy

X-band CW EPR spectra were obtained on a Bruker EMX spectrometer at 77 K in a liquid nitrogen immersion dewar using Bruker Win-EPR software (ver. 3.0). Samples were prepared as solutions (2 mM) in 2-methyltetrahydrofuran (2Me-THF) and rapidly cooled in liquid nitrogen to form a frozen glass. Spectra were simulated using the EasySpin[9] simulation toolbox (release 5.1.8) with Matlab 2016b.

Pulse EPR Spectroscopy

All pulse EPR and electron nuclear double resonance (ENDOR) experiments were aquired using a Bruker (Billerica, MA) ELEXSYS E580 pulse EPR spectrometer using a Bruker MD4 pulse ENDOR resonator for all X-band experiments and a Bruker D2 pulse ENDOR resonator for all Q-band (≈ 33.7 GHz) experiments. Temperature control was achieved using an ER 4118HV-CF5-L Flexline Cryogen-Free VT cryostat manufactured by ColdEdge (Allentown, PA) equipped with an Oxford Instruments Mercury ITC.

Pulse Q-band electron spin-echo detected EPR (ESE-EPR) field-swept spectra were acquired using the 2-pulse "Hahn-echo" sequence ($\pi/2 - \tau - \pi -$ echo) and subsequently, each field swept echo-detected EPR absorption spectrum was modified using a pseudo-modulation function[10] (modulation amplitude = 1 mT) to approximate the effect of field modulation and produce the CW-like 1st derivative spectrum.

Pulse X-band ENDOR was acquired using the Davies pulse sequence ($\pi - T_{RF} - \pi_{RF} - T_{RF} - \pi/2 - \tau - \pi -$ echo), where T_{RF} is the delay between mw pulses and RF pulses, π_{RF} is the length of the RF pulse and the RF frequency is randomly sampled during each pulse sequence.

In general, the ENDOR spectrum for a given nucleus with spin I= 1/2 (^{1}H, ^{31}P) or I= 3/2 ($^{95/97}$Mo and $^{35/37}$Cl) coupled to the S = ½ electron spin exhibits a doublet at frequencies

$$\nu_{\pm} = \left|\frac{A}{2} \pm \nu_N\right| \qquad \text{S1}$$

Where ν_N is the nuclear Larmor frequency and A is the hyperfine coupling. For nuclei with $I \geq 1$ ($^{95/97}$Mo, $^{35/37}$Cl), an additonal splitting of the $\nu_{\pm}$ manifolds is produced by the nuclear quadrupole interaction (P)

$$\nu_{\pm,m_I} = \left|\nu_N \pm \frac{3P(2m_I - 1)}{2}\right| \qquad \text{S2}$$

In the current study, these quadrupole transitions are not clearly resolved in any of the ENDOR spectra for either $^{95/97}$Mo or $^{35/37}$Cl. Particularly for $^{95/97}$Mo, these terms are likely vanishingly small in comparison to the strong hyperfine coupling, and thus are neglected in the spectral simulations.

Simulations of all EPR data were achieved using the EasySpin simulation toolbox (release 5.1.8) with Matlab 2016 using the following Hamiltonian:

$$\hat{H} = \mu_B \vec{B}_0 g \hat{S} + \mu_N g_N \vec{B}_0 \hat{I} + h\hat{S} \cdot \boldsymbol{A} \cdot \hat{I} \qquad \text{S3}$$

In this expression, the first term corresponds to the electron Zeeman interaction term where μ_B is the Bohr magneton, g is the electron spin g-value matrix with principle components g = [g_{xx} g_{yy} g_{zz}], and $\hat{S}$ is the electron spin operator; the second term corresponds to the nuclear Zeeman interaction term where μ_N is the nuclear magneton, g_N is the characteristic nuclear g-value for each nucleus (e.g. ^{1}H,^{31}P) and $\hat{I}$ is the nuclear spin operator; the third term corresponds to the electron-nuclear hyperfine term, where $\boldsymbol{A}$ is the hyperfine coupling tensor with principle components $\boldsymbol{A}$ = [A_{xx} A_{yy} A_{zz}].

EPR Spectra

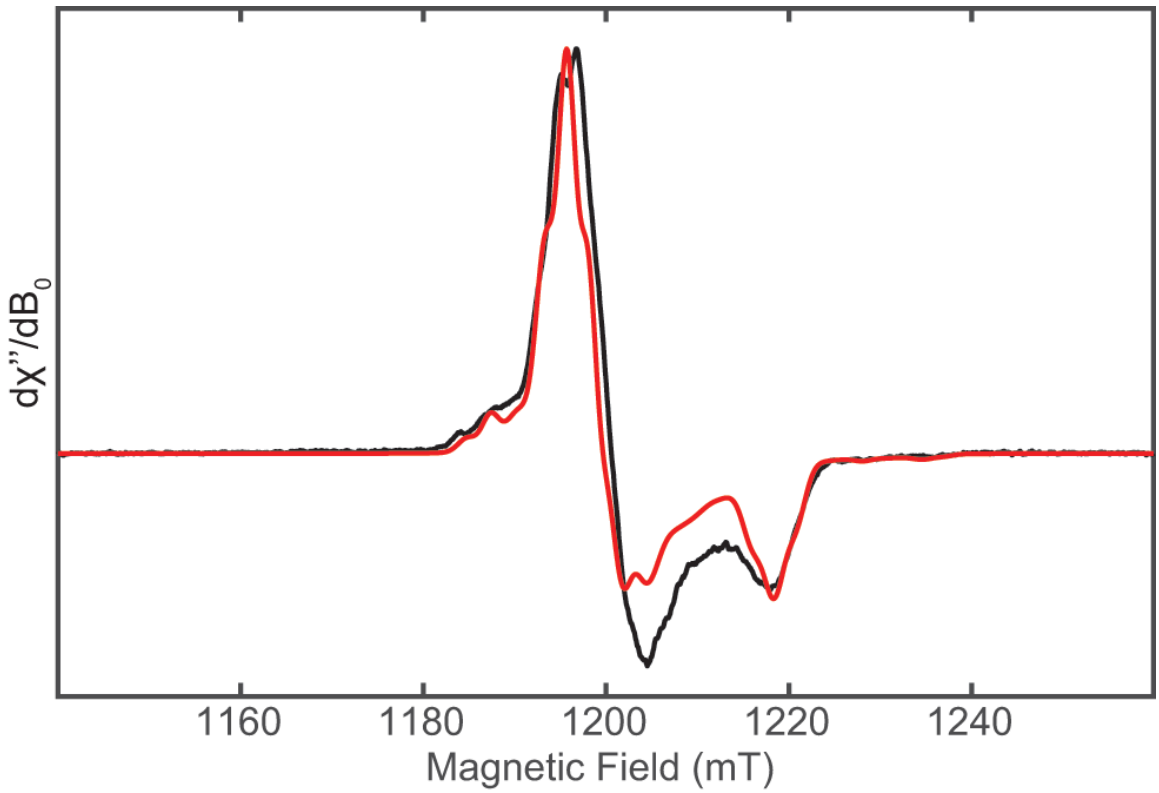

Figure S22—Q-band Pseudomodulated Electron Spin-Echo (ESE) detected EPR spectrum (black) of **3** in 2Me-THF with simulated CW EPR spectrum (red) using the same simulation parameters as for the X-band CW and ENDOR spectra. Pseudmodulation function amplitude = 1 mT. Experimental conditions: microwave frequency = 33.609 GHz; π pulse length = 160 ns; interpulse delay τ = 300ns; shot repetition time (srt) = 5 ms; temperature = 20 K.

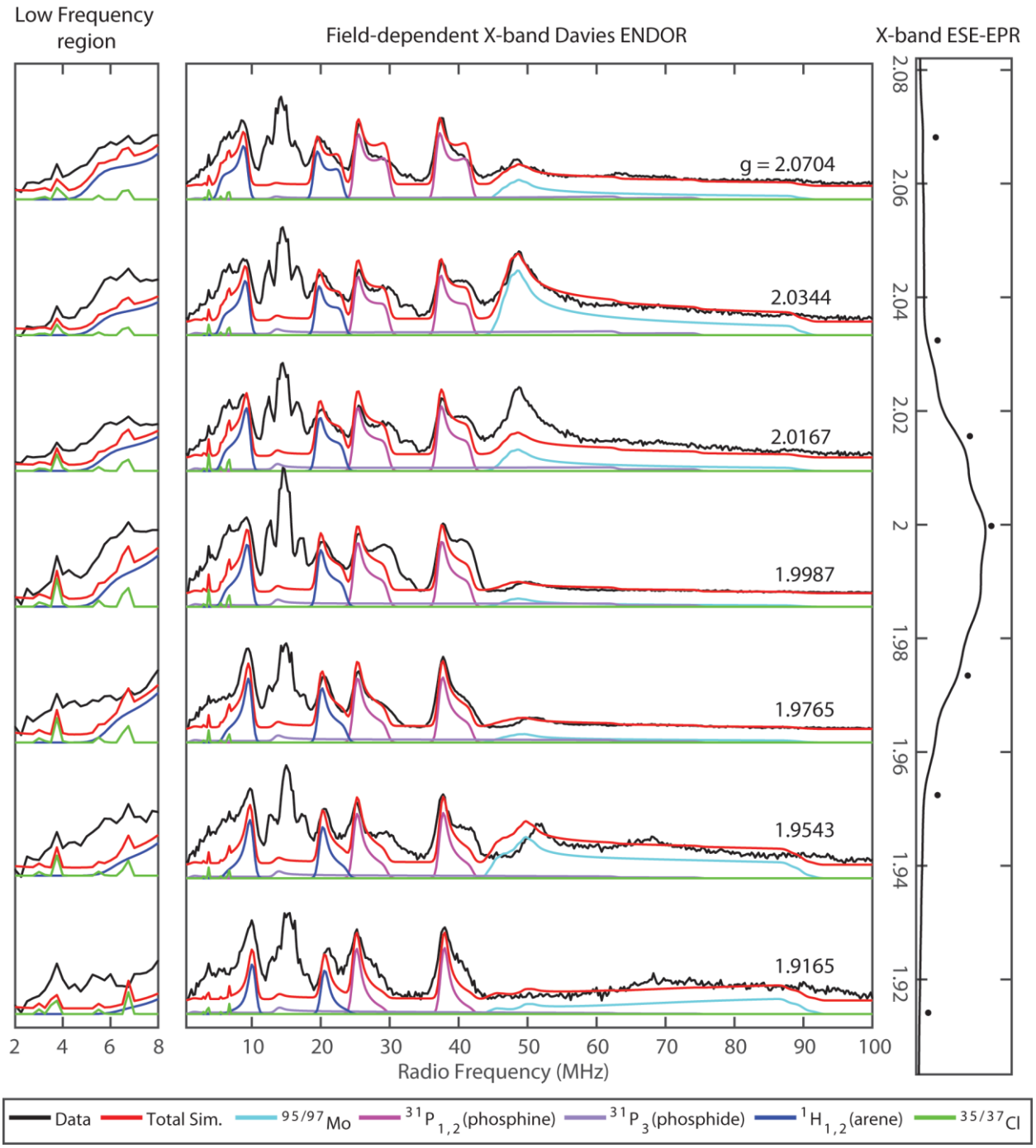

Figure S23—Field-dependent X-band Davies ENDOR spectra (black) of **3** in 2Me-THF and simulated ENDOR spectra of each hyperfine coupled nucleus (colored traces) using the same simulation parameters as for the X-band CW and ENDOR spectra. An enlargement of the low frequency region is offset to the left. Experimental conditions: microwave frequency = 9.724 GHz; MW π pulse length = 80 ns; RF π pulse length = 15 μs; interpulse delay τ = 240ns; T_{RF} delay = 2 μs; shot repitition time (srt) = 5 ms; temperature = 20.

Table S1—Absolute values of hyperfine coupling parameters for **3**, all units are in MHz.

Nucleus	x	y	z
$^{95/97}$Mo	94	94	178
Phosphine ^{31}P	62	72	63
Phosphide ^{31}P	15	138	15
Arene ^{1}H	10	18	10
$^{35/37}$Cl	10.5	10.5	10.5

*Estimation of spin density from hyperfine coupling parameters for **3***

Each hyperfine coupling tensor can be considered as the sum of an isotropic term, a_{iso}, which is the average value of the three principle components of the hyperfine tensor, and an anisotopic term dipolar term T_{obs}. These hyperfine values can be compared to calculated hyperfine values for a unit of spin in the appropriate orbital in order to obtain an estimate of the spin density at the nucleus in question.

Decomposition of $^{95/97}$Mo Hyperfine and estimation of spin density

The observed $^{95/97}$Mo Hyperfine coupling tensor is the sum of the isotropic term, a_{iso}, and an anisotropic term a_{aniso}. Here we will consider only the more abundant ^{95}Mo nucleus (15.92 %), though the analagous analysis could be approached by simply scaling the ^{95}Mo hyperfine by the ratio of the gyromagnetic ratios of ^{95}Mo and ^{97}Mo.

$$A(^{95}\text{Mo}) = [94, 94, 178]\ \text{MHz}$$

$$= a_{iso} + \boldsymbol{A}_{aniso} \qquad \text{S4}$$

$$= 122 + [-28\ -28\ 56]\ \text{MHz}$$

Taking $\left| a^0_{iso}(^{95}\text{Mo}) \right| = 1984$ MHz for a single electron in a 5s orbital of Mo,[11] the isotropic hyperfine coupling $a_{iso}(^{95}\text{Mo}) = 122$ MHz corresponds to a small 5s orbital density on Mo of $\rho_s \approx 0.06$ e$^-$. This is unsurprising considering the majority of unpaired spin resides within a valence d-orbital of xy parentage which gives rise to the sizable dipolar component. Taking a unit of unpaired spin in a d_{xy} orbital of Mo $\boldsymbol{A}^0_{d_{xy}}$= [-43.1 -43.1 86.2],[11] the anisotropic term $\boldsymbol{A}_{aniso}(^{95}\text{Mo}) = [-28\ -28\ 56]$ MHz corresponds to a $5d_{xy}$ orbital spin density of $\rho_{d_{xy}} \approx 0.65$ e$^-$. Between these two contributions, the total spin density at Mo is estimated to be $\rho_{Mo} \approx 0.71$ e$^-$, in reasonable agreement with the DFT-predicted Mulliken spin density of 0.774 e$^-$.

*Decomposition of terminal phosphide ^{31}P hyperfine and estimation of spin density for **3***

Following the procedures of Hoffman and coworkers for analysis of the ^{15}N hyperfine coupling in an Fe(V) nitride,[12] the highly anisotropic ^{31}P hyperfine coupling tensor measured for the terminal phosphide can also be decomposed to its constituent s- and p-orbital origins. In the case of this ^{31}P coupling, the relative signs of the individual principle components are not explicitly known, thus two cases must be considered,

$$A(^{31}\text{P}) = [15, 138, 15] \text{ or } [-15, 138, -15]\ \text{MHz}$$

$$= a_{iso} + \boldsymbol{T}_{obs}$$

= 56 + [-41, 82, -41] MHz or 36 + [-51, 102, -51] MHz

Taking $a^0_{iso}(^{31}\text{P})$ = 13308 MHz for a single electron in a 3*s* orbital, the isotropic hyperfine $a_{iso}(^{31}\text{P})$ = 56 or 36 MHz corresponds to a small 3s orbital density on the phosphide P of $\rho_s \approx 0.004$ e$^-$ or $\rho_s \approx 0.003$ e$^-$, respectively, either case indicating that the terminal phosphide can be treated as having a filled 3s orbital with little hybridization with p-orbitals containing unpaired spin density.

In the case of the phosphide, the dipolar term $\boldsymbol{T}_{obs}$ can be decomposed into two separate axial contributions: one local contribution, $\boldsymbol{T}^{x,y}{}_{loc}$, from spin density at P with its unique axis along an axis (x or y) orthogonal to the Mo-P bond vector, and a second component, $\boldsymbol{T}^{z}{}_{obs}$, with its unique axis parallel to the Mo-P bond vector. In turn, $\boldsymbol{T}^{z}{}_{obs}$ is a composite of the nonlocal contribution ($\boldsymbol{T}^{z}{}_{nloc}$) due to the through-space dipolar interaction between the ^{31}P nucleus and unpaired spin density at the Mo nucleus, and a local contribution ($\boldsymbol{T}^{z}{}_{loc}$) from spin density at P in a p-orbital with its unique axis parallel to the Mo-P bond vector. The nonlocal contribution $\boldsymbol{T}^{z}{}_{nloc}$ can be estimated using the point-dipole approximation:

$$\boldsymbol{T}^{z}{}_{nloc} = [-a, -a, 2a]; a = \frac{\rho_{Mo} g_e \mu_B g_n \mu_n}{r^3} \qquad \text{S5}$$

Using the crystallographically determined Mo-P distance (r = 2.092(1) Å) and $\rho_{Mo} \approx 0.71$, the spin density at Mo determined in the previous section, results in an estimation of $\boldsymbol{T}^{z}{}_{nloc} = [-2.5,\ -2.5,\ 5.0]$ MHz. Subtraction of this nonlocal contributon $\boldsymbol{T}^{z}{}_{nloc}$ from $\boldsymbol{T}_{obs}$ yields the sum of the local contributions:

$$\boldsymbol{T}_{loc} = \boldsymbol{T}_{obs} - \boldsymbol{T}^{z}{}_{nloc}$$

= [-38.5, 84.5, -46.0] or [-48.5, 104.5, -46.0]

$$= \boldsymbol{T}^{x,y}{}_{loc} + \boldsymbol{T}^{z}{}_{loc}$$

For both cases considered for $\boldsymbol{T}_{obs}$, $\boldsymbol{T}_{loc}$ can be uniquely decomposed into $\boldsymbol{T}^{x,y}{}_{loc} + \boldsymbol{T}^{z}{}_{loc}$ components with $\boldsymbol{T}^{z}{}_{loc}$ = [2.5, 2.5, -5.0] for both and $\boldsymbol{T}^{x,y}{}_{loc}$ = [-41, 82, -41] or [-51, 102, -51], respectively. Though a definitive asignment of the orientation of these hyperfine tensors relative to the molecular frame cannot be made from the current data, the uniaxial symmetry of both of these two $\boldsymbol{T}^{x,y}{}_{loc}$ tensors implies that in either case that only one p-orbital is contributing, with either ρ_{p_x} or $\rho_{p_y} \approx 0$. In the simulations presented, hyperfine and g-tensor principle coordinates are co-linear, and the most likely orientation of the g-tensor coordinate frame is with g_z parallel to the Mo-phosphide bond vector, while g_y is roughly aligned with the phosphine-Mo-phosphine vector. Taking a unit of unpaired spin in a p_y orbital of P $\boldsymbol{A}^{o}_{p_{x,y}}$= [-366.8 733.6 -366.8] MHz,[11] these two cases of $\boldsymbol{T}^{x,y}{}_{loc}$ correspond to a p-orbital spin density of $\rho_{p_y} \approx 0.11$ or 0.14 e$^-$, respectively. This significant unpaired spin in the p_y orbital of the terminal phosphide arises either from electron donation from filled orbitals on P to the partially filled d_{xy} orbital of Mo, or through spin polarization of the filled 3*p* orbitals on P by the same partially filled Mo d_{xy} orbital.

Absorbance Spectra

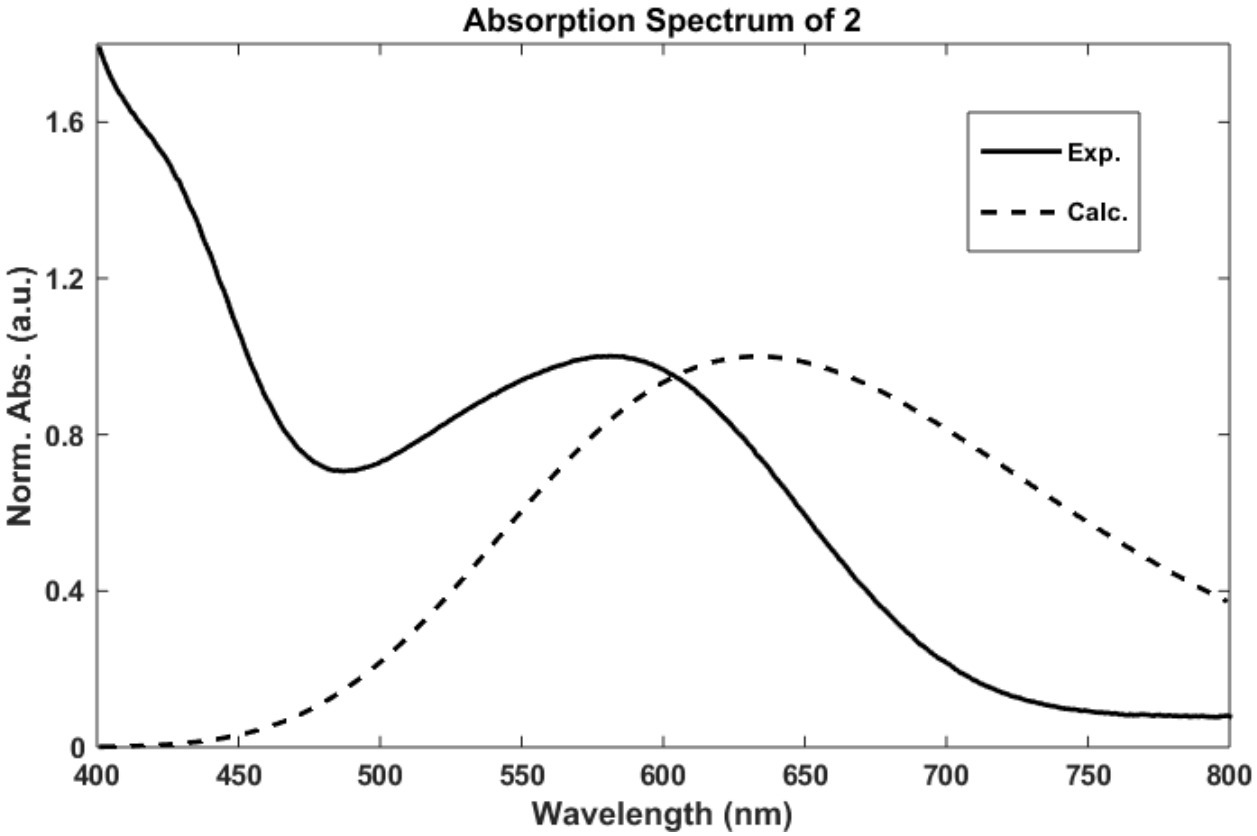

Figure S24—Experimental (solid) and TD-DFT calculated (dashed) UV-Vis spectra for terminal phosphide **2**. The data demonstrate reasonable agreement for the absorption maximum ($\Delta \approx 50$ nm)—with calculated 2a' → 3a'' and 2a' → 4a'' (Mo≡P N.B. to π^*) transitions at 613 and 561 nm, respectively.

Electrochemical Measurements

General Considerations

Electrochemical measurements were recorded with a Pine Instrument Company AFCBP1 bipotentiostat using the AfterMath software package. Cyclic Voltammograms (CVs) were recorded on a *ca.* 3 mmol solution of **2** in a 0.1 M [^{n}Bu$_4$N][PF$_6$] electrolyte solution in THF. A two-compartment cell was employed; a Ag wire pseudo-reference electrode was separated from a Pt wire counter and 3.0 mm glassy carbon disk working electrode by a fine porosity sintered glass frit. Reported potentials were referenced internally to cobaltacene/cobaltacenium and are reported versus ferrocene/ferrocenium (Fc/Fc$^+$). For low temperature measurements, the two compartment cell was cooled in a low form Dewar flask containing acetone. Dry ice was added as needed to maintain a temperature of -20 ± 3 °C, as measured with a -100 to 50 °C alcohol thermometer (VWR).

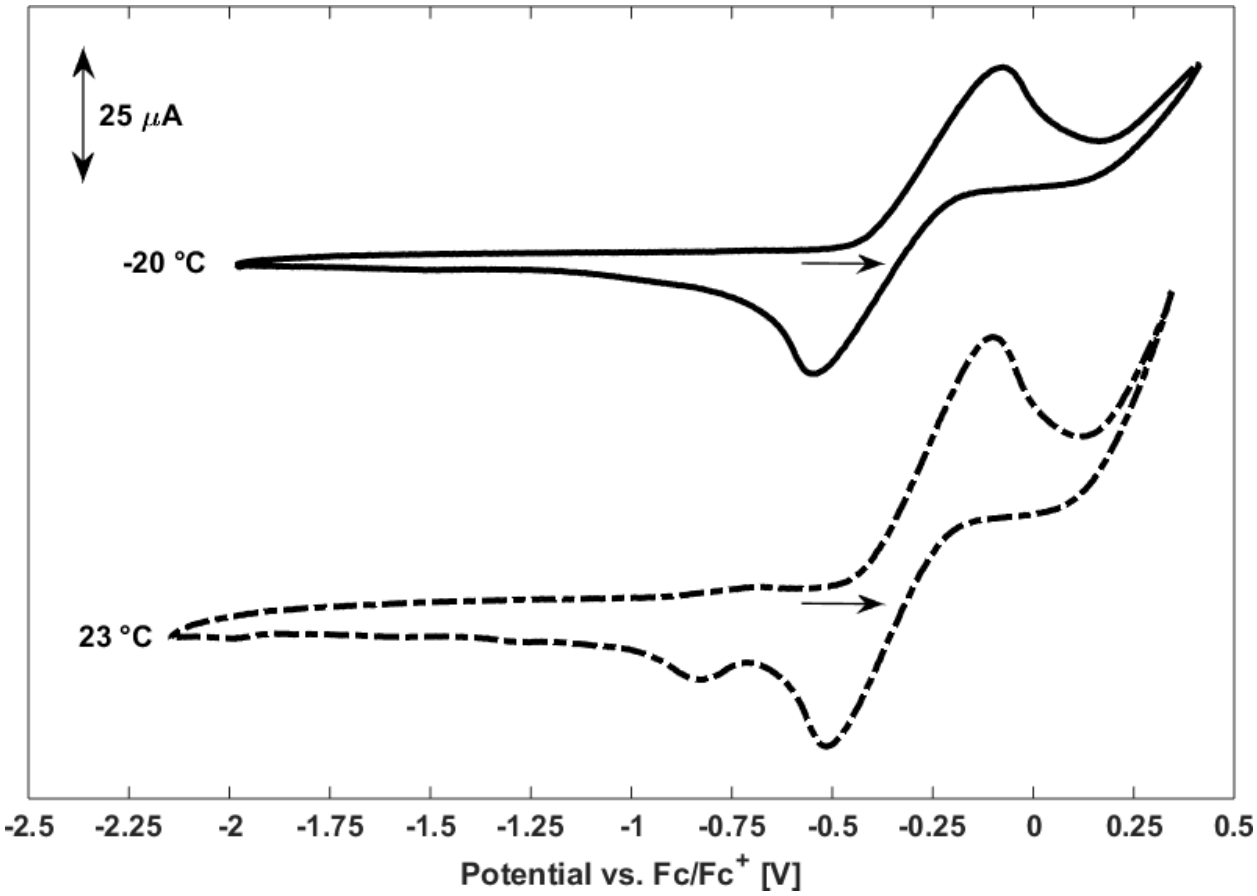

Figure S25—CVs of **2** in 0.1 M [^{n}BuN][PF$_6$] in THF recorded with a scan rate of 100 mV/s at -20 °C (solid) and 23 °C (dashed). Potentials are referenced to Fc/Fc+. The open circuit potential and scan direction are designated by the arrows under each voltammogram.

Though chemically reversible at -20 °C (*vide infra*), the Mo(IV)/Mo(V) redox couple of **2** demonstrates chemical irreversibility at room temperature. Upon scanning anodically, the low temperature CV shows a single return wave, corresponding to the reduction of *in situ* generated **3**. The room temperature CV has two cathodic features; one corresponding to reduction of **3**, and a second feature at -841 mV vs. Fc/Fc+. Despite being run under significantly more dilute conditions (*ca.* 20 fold more dilute), these data are

consistent with the reactivity observed from **3** upon chemical oxidation of **2** (a process proposed to be second order in [Mo]).

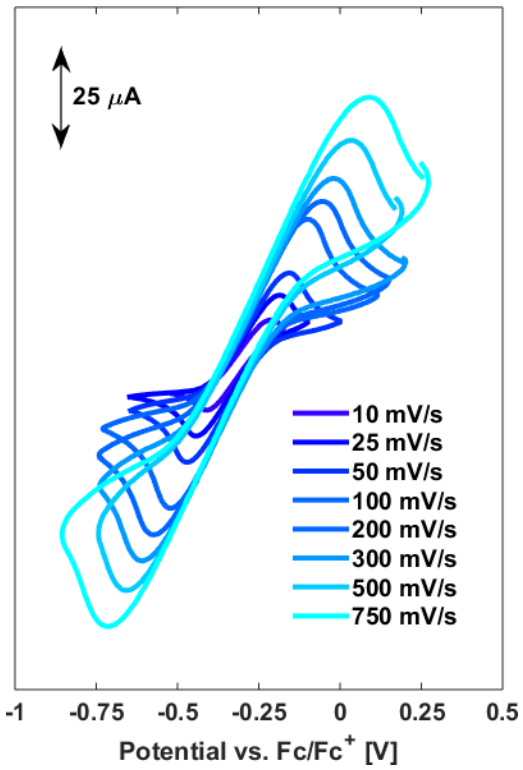

Figure S26—CVs corresponding to the Mo(IV)/Mo(V) redox couple of **2** in 0.1 M [^{n}BuN][PF_6] in THF recorded with variable scan rates at -20 °C.

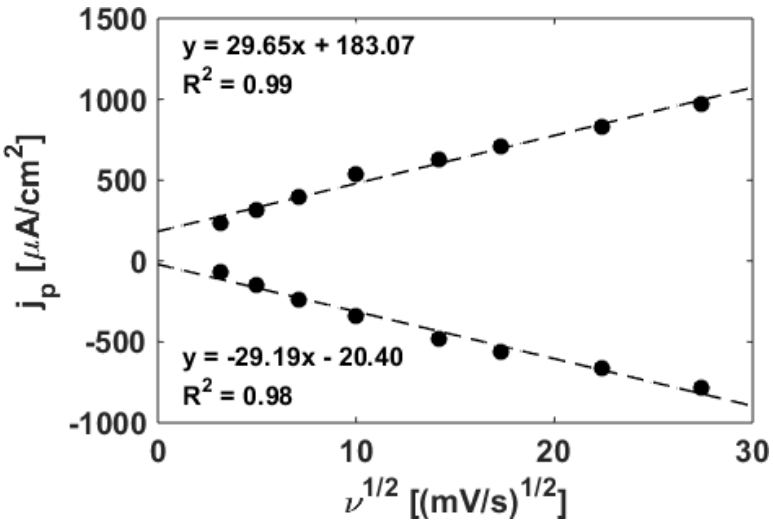

Figure S27—Current density dependence on the square root of the scan rate for the Mo(IV)/Mo(V) redox couple of **2** measured at -20 °C.

Computational Details

All calculations were performed with DFT as implemented in Gaussian 09 Revision C.01.[13] Geometry optimizations and electronic structure calculations were performed with revised TPSS exchange and correlation functionals.[14] The LANL2DZ basis set was used for all atoms.[15] No solvent corrections were employed. All optimizations were performed ignoring molecular symmetry—crystallographic coordinates were used as a starting point. Energetic minima were confirmed with subsequent frequency calculations which did not return imaginary frequencies. Structures optimized in this manner showed good agreement with bond lengths and angles determined via single crystal X-ray diffraction (Table S1). The TD-DFT calculated absorption spectrum of **2** demonstrated reasonable agreement with the experimentally determined UV-Vis spectrum (Figure S24). Molecular orbital and spin density illustrations were generated using GaussView, the GUI component of the Gaussian software package, and depicted with 0.05 e/Å^3 or 0.001 e/Å^3 isosurface values, respectively.

Table S2—Comparison of Experimental and Calculated Structural Metrics for **2** and **3**.

	2			**3**		
	Exp.	**Calc.**	Δ	**Exp.**	**Calc.**	Δ
Mo1–P1	2.5959(3)	2.644	-0.05	2.6092(8)	2.667	-0.06
Mo1–P2	2.5922(3)	2.644	-0.05	2.6226(8)	2.667	-0.04
Mo1–P3	2.1003(3)	2.150	-0.05	2.092(1)	2.141	-0.05
Mo1–Cl1	2.4358(3)	2.508	-0.07	2.3411(9)	2.425	-0.08
Mo1–C2	2.261(1)	2.277	-0.02	2.465(3)	2.476	-0.01
Mo1–C3	2.255(1)	2.277	-0.02	2.471(3)	2.476	-0.01
C1–C2	1.453(2)	1.467	-0.01	1.413(4)	1.438	-0.03
C2–C3	1.433(2)	1.462	-0.03	1.402(4)	1.428	-0.03
C3–C4	1.453(2)	1.467	-0.01	1.414(4)	1.438	-0.02
C4–C5	1.361(2)	1.389	-0.03	1.387(5)	1.411	-0.02
C5–C6	1.435(2)	1.446	-0.01	1.401(5)	1.420	-0.02
C6–C1	1.359(2)	1.389	-0.03	1.388(5)	1.411	-0.02
∠P1–Mo1–P2	162.3(1)	160.8	1.5	161.8(1)	161.3	0.5
∠P1–Mo1–P3	97.5(1)	97.4	0.1	96.8(1)	98.1	-1.3
∠P2–Mo1–P3	96.2(1)	97.4	-1.2	98.2(1)	98.1	0.1
∠P1–Mo1–Cl1	82.0(1)	82.2	-0.2	82.9(1)	83.6	-0.7
∠P2–Mo1–Cl1	83.5(1)	82.2	1.3	83.6(1)	83.6	0
∠P3–Mo1–Cl1	105.7(1)	105.5	0.2	103.0(1)	103.0	0

Table S3—Computed Mulliken Spin Densities and Experimental Isotropic Hyperfine Coupling Constants for **3**.

	Calculated Mulliken Spin Density (e^-)	**A_{iso} (MHz)**
Mo1	0.774	122.0
Cl1	0.067	10.5
H2	0.018	12.7
H3	0.018	12.7

Cartesian Coordinates for 2

Mo	0.000000	-0.619000	-0.345000
Cl	0.000000	-2.271000	1.542000
P	2.607000	-0.664000	0.093000
P	-2.607000	-0.664000	0.093000
P	0.000000	-1.799000	-2.142000
C	-0.731000	1.368000	-1.184000
H	-1.265000	1.122000	-2.101000
C	3.594000	0.930000	-0.282000
C	5.004000	0.904000	-0.420000
H	5.535000	-0.047000	-0.438000
C	3.033000	-0.915000	1.983000
H	2.474000	-1.829000	2.229000
C	1.436000	2.247000	-0.244000
C	-3.653000	-2.043000	-0.782000
H	-4.672000	-1.940000	-0.377000
C	0.731000	1.368000	-1.184000
H	1.265000	1.122000	-2.101000
C	-5.091000	3.344000	-0.481000
H	-5.660000	4.271000	-0.557000
C	0.723000	3.071000	0.617000
H	1.254000	3.702000	1.332000
C	2.922000	2.193000	-0.277000
C	-5.751000	2.097000	-0.532000
H	-6.834000	2.049000	-0.648000
C	-3.594000	0.930000	-0.282000
C	5.751000	2.097000	-0.532000
H	6.834000	2.049000	-0.648000
C	2.435000	0.256000	2.802000
H	2.925000	1.209000	2.554000
H	2.582000	0.063000	3.876000
H	1.356000	0.356000	2.623000
C	-0.723000	3.071000	0.617000
H	-1.254000	3.702000	1.332000
C	3.653000	-2.043000	-0.782000
H	4.672000	-1.940000	-0.377000
C	-3.688000	3.386000	-0.359000
H	-3.165000	4.343000	-0.363000
C	3.109000	-3.444000	-0.407000
H	3.148000	-3.626000	0.676000
H	3.717000	-4.214000	-0.908000
H	2.065000	-3.559000	-0.730000
C	-3.033000	-0.915000	1.983000
H	-2.474000	-1.829000	2.229000
C	-1.436000	2.247000	-0.244000
C	-2.922000	2.193000	-0.277000
C	-2.435000	0.256000	2.802000
H	-1.356000	0.356000	2.623000
H	-2.582000	0.063000	3.876000
H	-2.925000	1.209000	2.554000
C	3.688000	3.386000	-0.359000
H	3.165000	4.343000	-0.363000
C	-5.004000	0.904000	-0.420000
H	-5.535000	-0.047000	-0.438000
C	4.534000	-1.111000	2.301000
H	4.965000	-1.979000	1.783000
H	4.644000	-1.287000	3.384000
H	5.123000	-0.218000	2.048000
C	-3.704000	-1.832000	-2.315000
H	-4.129000	-0.854000	-2.581000
H	-4.329000	-2.616000	-2.769000
H	-2.698000	-1.906000	-2.754000
C	3.704000	-1.832000	-2.315000
H	2.698000	-1.906000	-2.754000
H	4.329000	-2.616000	-2.769000
H	4.129000	-0.854000	-2.581000
C	-4.534000	-1.111000	2.301000
H	-5.123000	-0.218000	2.048000
H	-4.644000	-1.287000	3.384000
H	-4.965000	-1.979000	1.783000
C	-3.109000	-3.444000	-0.407000
H	-2.065000	-3.559000	-0.730000
H	-3.717000	-4.214000	-0.908000
H	-3.148000	-3.626000	0.676000
C	5.091000	3.344000	-0.481000
H	5.660000	4.271000	-0.55700

Cartesian Coordinates for 3

Mo	-0.000000	-0.678000	-0.333000
Cl	-0.000000	-2.406000	1.369000
P	2.631000	-0.669000	0.101000
P	-2.631000	-0.669000	0.101000
P	0.000000	-1.800000	-2.157000
C	-0.714000	1.500000	-1.269000
H	-1.257000	1.095000	-2.120000
C	3.590000	0.936000	-0.279000
C	5.002000	0.909000	-0.396000
H	5.537000	-0.039000	-0.392000
C	2.992000	-0.923000	2.001000
H	2.455000	-1.855000	2.225000
C	1.437000	2.272000	-0.295000
C	-3.666000	-2.051000	-0.785000
H	-4.681000	-1.941000	-0.373000
C	0.714000	1.500000	-1.269000
H	1.257000	1.095000	-2.120000
C	-5.089000	3.349000	-0.485000
H	-5.658000	4.274000	-0.562000
C	0.710000	3.084000	0.601000
H	1.245000	3.689000	1.332000
C	2.922000	2.199000	-0.299000
C	-5.748000	2.102000	-0.511000
H	-6.831000	2.054000	-0.608000
C	-3.590000	0.936000	-0.279000
C	5.748000	2.102000	-0.511000
H	6.831000	2.054000	-0.608000
C	2.345000	0.233000	2.805000
H	2.833000	1.194000	2.585000
H	2.458000	0.033000	3.880000
H	1.270000	0.322000	2.593000
C	-0.710000	3.084000	0.601000
H	-1.245000	3.689000	1.332000
C	3.666000	-2.051000	-0.785000
H	4.681000	-1.941000	-0.373000
C	-3.684000	3.394000	-0.379000
H	-3.167000	4.352000	-0.401000
C	3.132000	-3.457000	-0.413000
H	3.153000	-3.638000	0.670000
H	3.766000	-4.215000	-0.897000
H	2.101000	-3.600000	-0.763000
C	-2.992000	-0.923000	2.001000
H	-2.455000	-1.855000	2.225000
C	-1.437000	2.272000	-0.295000
C	-2.922000	2.199000	-0.299000
C	-2.345000	0.233000	2.805000
H	-1.270000	0.322000	2.593000
H	-2.458000	0.033000	3.880000
H	-2.833000	1.194000	2.585000
C	3.684000	3.394000	-0.379000
H	3.167000	4.352000	-0.401000
C	-5.002000	0.909000	-0.396000
H	-5.537000	-0.039000	-0.392000
C	4.491000	-1.086000	2.350000
H	4.956000	-1.934000	1.830000
H	4.576000	-1.281000	3.430000
H	5.063000	-0.175000	2.131000
C	-3.722000	-1.830000	-2.315000
H	-4.137000	-0.847000	-2.579000
H	-4.362000	-2.602000	-2.766000
H	-2.724000	-1.923000	-2.769000
C	3.722000	-1.830000	-2.315000
H	2.724000	-1.923000	-2.769000
H	4.362000	-2.602000	-2.766000
H	4.137000	-0.847000	-2.579000
C	-4.491000	-1.087000	2.350000
H	-5.063000	-0.175000	2.131000
H	-4.576000	-1.281000	3.430000
H	-4.956000	-1.934000	1.830000
C	-3.132000	-3.457000	-0.413000
H	-2.101000	-3.600000	-0.763000
H	-3.766000	-4.215000	-0.897000
H	-3.153000	-3.638000	0.670000
C	5.089000	3.349000	-0.485000
H	5.658000	4.274000	-0.562000

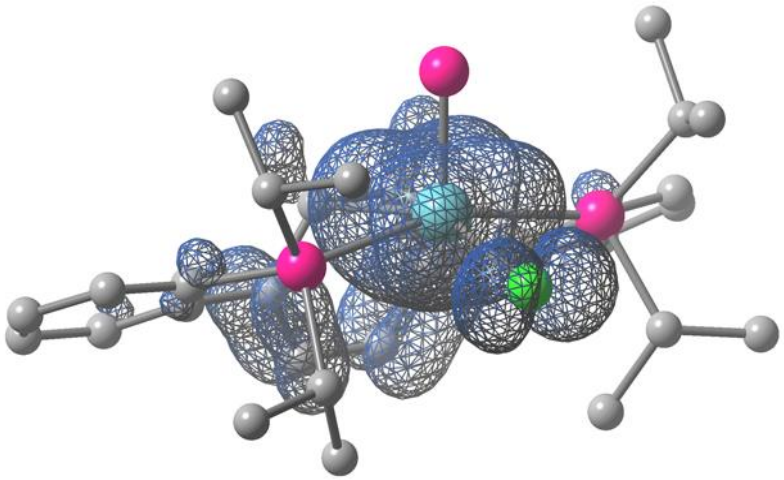

Figure S28—Spin density plot (0.001 e/Å^3 isocontours) of phosphide cation **3**.

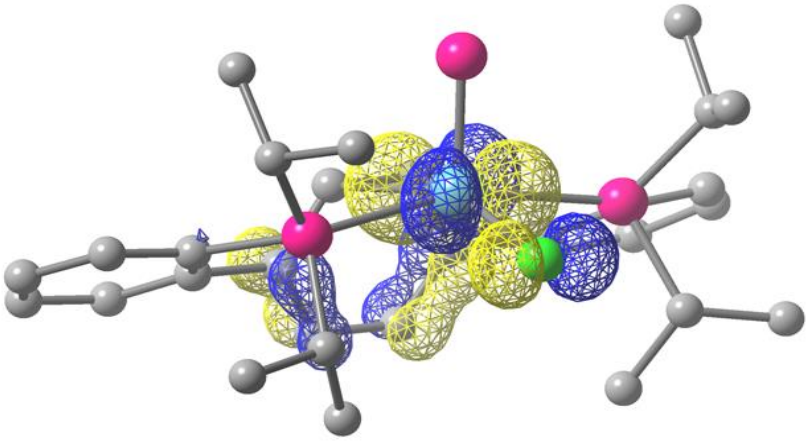

Figure S29—Calculated SOMO (0.05 e/Å^3 isocontours) for phosphide cation **3**.

Crystallographic Information

CCDC deposition numbers 1571924-1571926 contain the supplementary crystallographic data for this paper. These data can be obtained free of charge from The Cambridge Crystallographic Data Centre via www.ccdc.cam.ac.uk/data_request/cif.

Refinement Details

In each case, crystals were mounted on a MiTeGen loop using Paratone oil, then placed on the diffractometer under a nitrogen stream. Low temperature (100 K) X-ray data were obtained on a Bruker D8 VENTURE Kappa Duo PHOTON 100 CMOS based diffractometer (Mo $I_{\mu}S$ HB micro-focus sealed X-ray tube, K_{α} = 0.71073 Å). All diffractometer manipulations, including data collection, integration, and scaling were carried out using the Bruker APEXIII software.[16] Absorption corrections were applied using SADABS.[17] Space groups were determined on the basis of systematic absences and intensity statistics and the structures were solved in the Olex 2 software interface[18] by intrinsic phasing using XT (incorporated into SHELXTL)[19] and refined by full-matrix least squares on F^2. All non-hydrogen atoms were refined using anisotropic displacement parameters. Hydrogen atoms were placed in the idealized positions and refined using a riding model, unless noted otherwise. The structures were refined (weighed least squares refinement on F^2) to convergence. Graphical representations of structures with 50% probability thermal ellipsoids were generated using the Diamond 3 visualization software.[20]

Table S4—Crystal and refinement data for complexes **2 - 4**.

	2	**3**	**4**
CCDC Number[21]	1571924	1571925	1571926
Empirical formula	$C_{30}H_{40}ClMoP_3$	$C_{71.08}H_{74.70}BClF_{24}MoO_{2.27}P_3$	$C_{35}H_{46}ClF_3MoN_2O_3P_2S$
Formula weight	624.92	1656.39	825.13
T (K)	100	100	100
a, Å	9.3388(5)	12.6893(4)	8.4978(5)
b, Å	15.0643(8)	16.9145(5)	13.3117(9)
c, Å	21.1092(11)	19.5016(6)	16.8759(11)
α, °	90	108.333(2)	75.595(2)
β, °	98.942(2)	100.223(2)	85.718(2)
γ, °	90	101.417(2)	76.193(2)
Volume, Å^3	2933.6(3)	3763.1(2)	1795.3(2)
Z	4	2	2
Crystal system	Monoclinic	Triclinic	Triclinic
Space group	$P2_1/n$	$P\bar{1}$	$P\bar{1}$
d_{calc}, g/cm^3	1.415	1.462	1.526
θ range, °	2.589 to 33.145	2.470 to 79.676	2.269 to 39.789
μ, mm^{-1}	0.720	3.274	0.641
Abs. Correction	Semi-empirical	Semi-empirical	Semi-empirical
GOF	1.029	1.059	0.800
R_1 ,[a] wR_2 [b] [I>2 σ(I)]	0.0243, 0.0528	0.0562, 0.1390	0.0564, 0.1271
Radiation Type	Mo K_α	Cu K_α	Mo K_α

[a] $R_1 = \sum||F_o| - |F_c||/\sum|F_o|$. [b] $wR_2 = [\sum[w(F_o^2-F_c^2)^2]/\sum[w(F_o^2)^2]^{1/2}$.

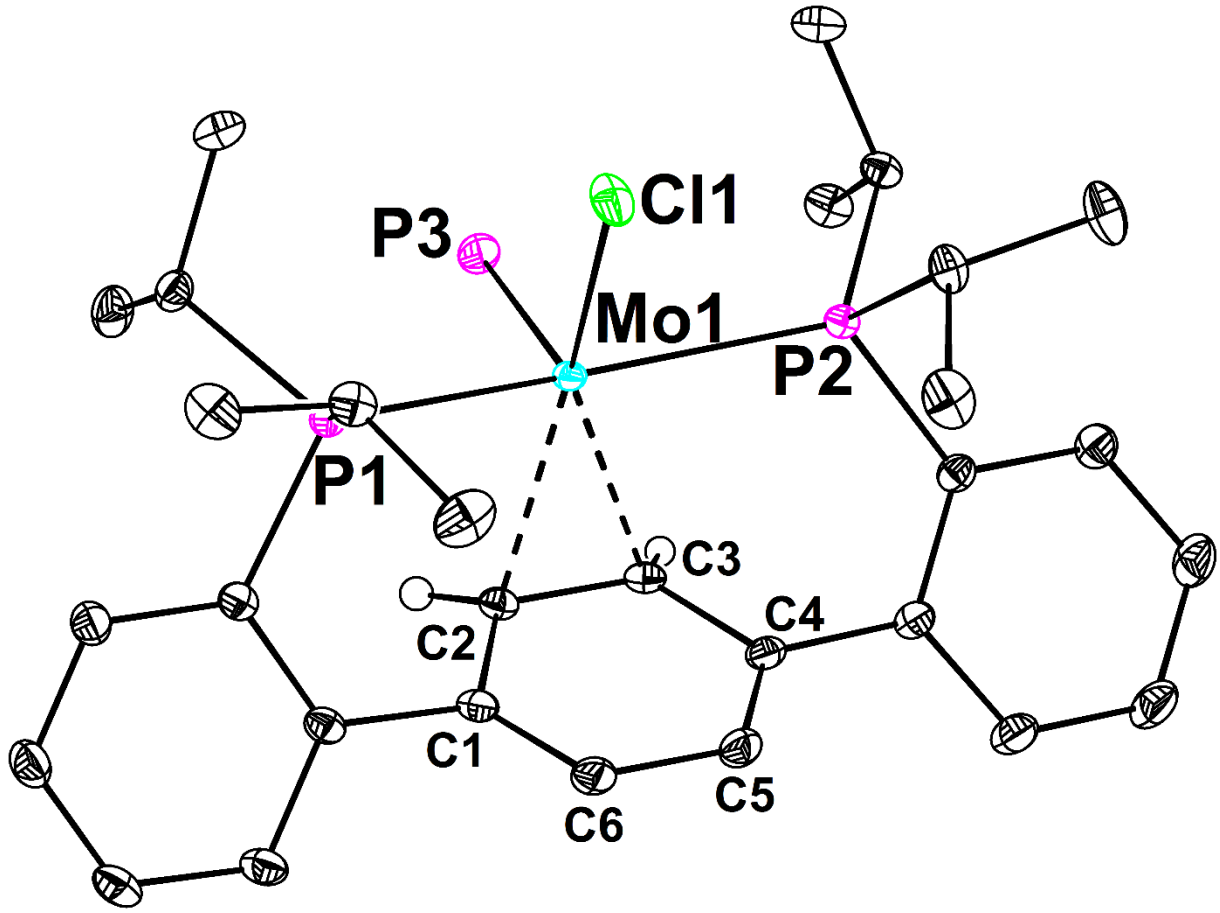

Figure S30—Structural drawing of **2** with 50% probability anisotropic displacement ellipsoids**.** Selected H-atoms are omitted for clarity.

Special Refinement Details:

The structure was of sufficient quality that the coordinates of the hydrogen atoms attached to both C2 and C3 were found in the difference map and refined freely. The η^2 metal-arene interaction results in a significant displacement of these H-atoms from their idealized positions.

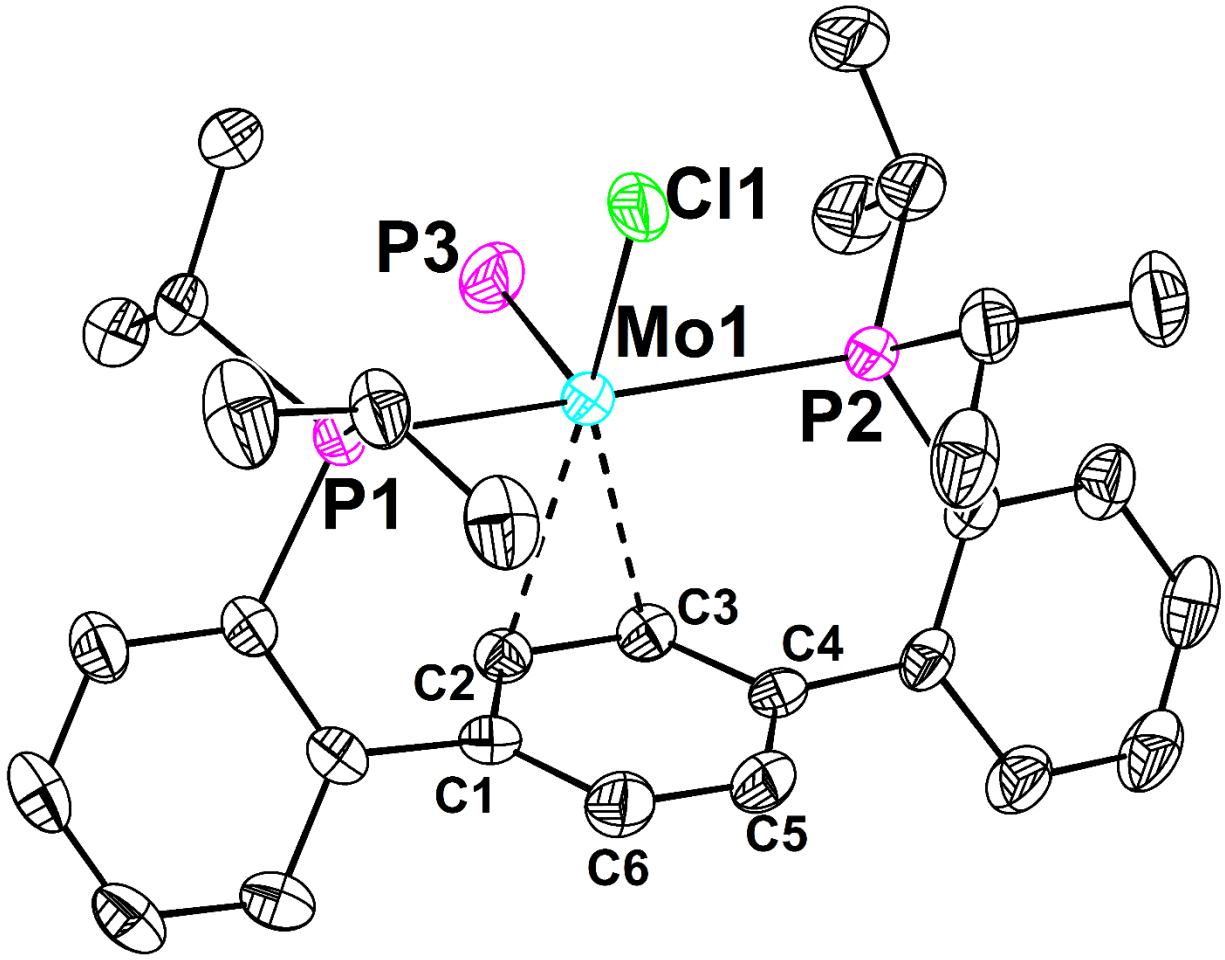

Figure S31—Structural drawing of **3** with 50% probability anisotropic displacement ellipsoids. H-atoms, the outer sphere BAr^{F}_{24} anion, and Et_2O solvate molecules are omitted for clarity.

Special Refinement Details:

One of the phosphine isopropyl groups (C28 through C30) was positionally disordered but was satisfactorily modeled over two positions in a 64:36 ratio. The 1,2 and 1,3 distances of the disordered group were restrained to be equivalent and enhanced rigid bond restraints were applied. Several of the CF_3 groups of the BAr^{F}_{24} counterion likewise displayed positional disorder. These groups were satisfactorily modeled over two (F4 through F6 [57:43], F7 through F9 [63:37], F10 through F12 [54:46], F13 through F15 [27:73], and F19 through F22 [49:51]) or three (F22 through F24 [20:33:47]) positions and refined with enhanced rigid bond restraints. Additionally, the most rotationally disordered CF_3 group (F13 through F15) was refined with the 1,2 and 1,3 distances to be equivalent; similarity restraints on U_{ij} and rigid bond restraints were likewise applied.

Highly disordered Et_2O solvent molecules were present in the crystal packing voids. Rather than employing a SQUEEZE operation, the density attributed to these solvate molecules was modeled discretely with 1,2 and 1,3 distance and enhanced rigid bond restraints. A total of 2.3 Et_2O molecules were modeled, giving rise to the non-integer unit cell contents.

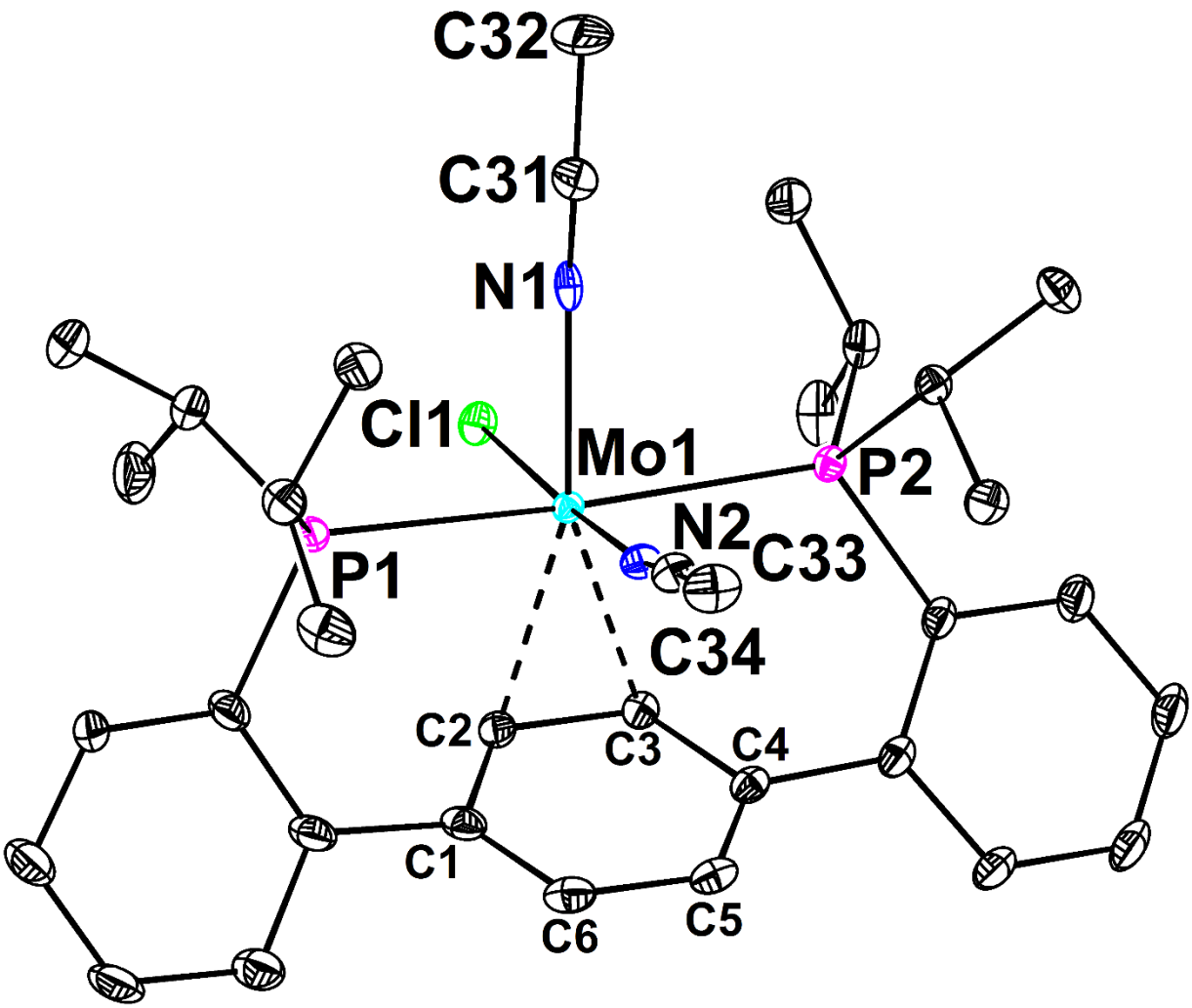

Figure S32—Structural drawing of **4** with 50% probability anisotropic displacement ellipsoids**.** H-atoms and the outer sphere triflate counterion are omitted for clarity.

Special Refinement Details:

One of the phenylene linkers (C9 through C12) demonstrated positional disorder but was satisfactorily modeled over two positions and refined without restraints. The triflate counterion (C35, F1 through F3, S1, and O1 through O3) was likewise positionally disordered. This anion was satisfactorily modeled over three positions in a 22:34:44 ratio and refined with 1,2 and 1,3 distance and enhanced rigid bond restraints.

References

(1) Pangborn, A. B.; Giardello, M. A.; Grubbs, R. H.; Rosen, R. K.; Timmers, F. J. *Organometallics* **1996**, *15*, 1518.
(2) Buss, J. A.; Edouard, G. A.; Cheng, C.; Shi, J.; Agapie, T. *J. Am. Chem. Soc.* **2014**, *136*, 11272.
(3) Velian, A.; Nava, M.; Temprado, M.; Zhou, Y.; Field, R. W.; Cummins, C. C. *J. Am. Chem. Soc.* **2014**, *136*, 13586.
(4) Freeman, P. K.; Hutchinson, L. L. *J. Org. Chem.* **1983**, *48*, 879.
(5) Burg, A. B.; Slota, P. J. *J. Am. Chem. Soc.* **1958**, *80*, 1107.
(6) Heinekey, D. M.; Radzewich, C. E. *Organometallics* **1998**, *17*, 51.
(7) Adhikari, D.; Mossin, S.; Basuli, F.; Huffman, J. C.; Szilagyi, R. K.; Meyer, K.; Mindiola, D. J. *J. Am. Chem. Soc.* **2008**, *130*, 3676.
(8) Fulmer, G. R.; Miller, A. J. M.; Sherden, N. H.; Gottlieb, H. E.; Nudelman, A.; Stoltz, B. M.; Bercaw, J. E.; Goldberg, K. I. *Organometallics* **2010**, *29*, 2176.
(9) Stoll, S.; Schweiger, A. *J. Magn. Reson.* **2006**, *178*, 42.
(10) Hyde, J. S.; Pasenkiewicz-Gierula, M.; Jesmanowicz, A.; Antholine, W. E. *Appl. Magn. Reson.* **1990**, *1*, 483.
(11) Morton, J. R.; Preston, K. F. *J. Magn. Reson.* **1978**, *30*, 577.
(12) Cutsail III, G. E.; Stein, B. W.; Subedi, D.; Smith, J. M.; Kirk, M. L.; Hoffman, B. M. *J. Am. Chem. Soc.* **2014**, *136*, 12323.
(13) Gaussian 09, Revision C.01, Frisch, M. J.; Trucks, G. W.; Schlegel, H. B.; Scuseria, G. E.; Robb, M. A.; Cheeseman, J. R.; Scalmani, G.; Barone, V.; Mennucci, B.; Petersson, G. A.; Nakatsuji, H.; Caricato, M.; Li, X.; Hratchian, H. P.; Izmaylov, A. F.; Bloino, J.; Zheng, G.; Sonnenberg, J. L.; Hada, M.; Ehara, M.; Toyota, K.; Fukuda, R.; Hasegawa, J.; Ishida, M.; Nakajima, T.; Honda, Y.; Kitao, O.; Nakai, H.; Vreven, T.; Montgomery, Jr., J. A.; Peralta, J. E.; Ogliaro, F.; Bearpark, M.; Heyd, J. J.; Brothers, E.; Kudin, K. N.; Staroverov, V. N.; Kobayashi, R.; Normand, J.; Raghavachari, K.; Rendell, A.; Burant, J. C.; Iyengar, S. S.; Tomasi, J.; Cossi, M.; Rega, N.; Millam, J. M.; Klene, M.; Knox, J. E.; Cross, J. B.; Bakken, V.; Adamo, C.; Jaramillo, J.; Gomperts, R.; Stratmann, R. E.; Yazyev, O.; Austin, A. J.; Cammi, R.; Pomelli, C.; Ochterski, J. W.; Martin, R. L.; Morokuma, K.; Zakrzewski, V. G.; Voth, G. A.; Salvador, P.; Dannenberg, J. J.; Dapprich, S.; Daniels, A. D.; Farkas, Ö.; Foresman, J. B.; Ortiz, J. V.; Cioslowski, J.; Fox, D. J. Gaussian, Inc., Wallingford CT, 2009.
(14) a) Perdew, J. P.; Ruzsinszky, A.; Csonka, G. I.; Constantin, L. A.; Sun, J. *Phys. Rev. Lett.* **2011**, *106*, 179902; b) Perdew, J. P.; Ruzsinszky, A.; Csonka, G. I.; Constantin, L. A.; Sun, J. *Phys. Rev. Lett.* **2009**, *103*, 026403.
(15) a) Wadt, W. R.; Hay, P. J. *J. Chem. Phys.* **1985**, *82*, 284; b) Hay, P. J.; Wadt, W. R. *J. Chem. Phys.* **1985**, *82*, 299; c) Hay, P. J.; Wadt, W. R. *J. Chem. Phys.* **1985**, *82*, 270; d) Dunning, T. H.; Hay, P. J. In *Methods of Electronic Structure Theory*; Schaefer, H. F., Ed.; Springer US: Boston, MA, 1977, p 1.
(16) APEX3, Version 1 User Manual, M86-EXX229, Bruker Analytical X-ray Systems, Madison, WI, May 2016.
(17) Sheldrick, G.M. "SADABS (version 2008/1): Program for Absorption Correction for Data from Area Detector Frames", University of Göttingen, 2008.
(18) Dolomanov, O. V.; Bourhis, L. J.; Gildea, R. J.; Howard, J. A. K.; Puschmann, H. *J. Appl. Crystallogr.* **2009**, *42*, 339.
(19) Sheldrick, G.M. *Acta Cryst.* **2008**, A64, 112-122.
(20) Brandenburg, K. (1999). DIAMOND. Crystal Impact GbR, Bonn, Germany.
(21) Crystallographic data have been deposited at the CCDC, 12 Union Road, Cambridge CB2 1EZ, UK and copies can be otained on request, free of charge, by quoting the publication citation and the respective deposition numbers.